Reduction of Cogging Forces in a Double Sided Tubular Linear Permanent Magnet Generator Used for Ocean Wave Energy Conversion

Rael Schmulian

A dissertation submitted to the Faculty of Engineering and the Built Environment, University of the Witwatersrand, Johannesburg, in fulfilment of the requirements for the degree of Master of Science in Engineering.

Johannesburg, 2012

Declaration

I declare that this dissertation is my own, unaided work, other than where specifically acknowledged. It is being submitted for the degree of Master of Science in Engineering in the University of the Witwatersrand, Johannesburg. It has not been submitted before for any degree or examination in any other university.

Signed this _____ day of _____ 2012

_____

Rael Schmulian

Abstract

An increased awareness of the environment and the growing energy needs of countries like China and India have accelerated the search for sustainable alternatives to fossil fuel energy sources. Generating electricity from ocean waves is a viable alternative. This is because energy densities are sufficient to supplement the grid and thus make it economically viable. The seasonal supply profile also matches the demand profile. There are currently many different devices operating on different principles, the most promising of these is the oscillating body device using a linear generator.

Linear generators are able to convert linear motion into electrical energy without the need for intermediate gears, screws or crank shafts. This increases the overall efficiency and makes the device more reliable. Static force simulations were done on a novel linear generator design. The generator combines the duel air-gap of a double sided topology with the encapsulation of the magnetic field in a tubular topology. This results in an increased force density, but also large cogging forces. The cogging forces consist of end-effects cogging forces that are caused by the interaction of the Permanent Magnets (PMs) with the stator ends, as well as cogging forces which are due to the interaction of the PMs and stator slots. The topic of this thesis is to find suitable methods of reducing the cogging forces.

The end-effect forces were reduced by changing the stator length and altering the stator ends shape. Creating a quadratic b'ezier curve end shape and optimising the stator length reduced the end-effect cogging force from 630 N to 7 N. The slot cogging forces were reduced by dividing the PMs into two sections and to shift the outer PMs by one slot pitch relative to the inner PMs. This resulted in a decrease from 663 N to 25 N. However, a compromise needs to be made between reducing the cogging forces and not reducing the machine performance. Increasing the stator length increases the machine volume and dividing the magnets reduces the thrust force. This needs to be taken into account when designing a new machine.

Acknowledgements

Firstly, I would like to thank my parents, whom have encouraged me and given me endless opportunities. I would also like to thank my supervisor, Professor Cronje, as I have tested his patience until the last moment. Lastly but definitely not least, I would like to thank my girlfriend, Kim, who has stood by my side, which I appreciate it a lot.

This research would not have been possible without financial assistance from the South African National Energy Research Institute (SANERI).

Contents

List of Figures

List of Tables

List of Symbols

δ	Difference between the stator length and the nearest integer multiple of pole pitches.
τ	Pole pitch.
F_{cn}	Fourier cosine coefficient.
F_{sn}	Fourier sine coefficient.
L_s	Length of the stator.

Chapter 1

Introduction

Growing environmental concerns and the rapid increase in energy consumption have accelerated the search for alternative energy sources. Recent developments such as the explosive economic growth in China and India have put stress on the planet's finite fossil fuel supply. Traditional renewable energy sources such as photo voltaic (PV) solar and wind can only be used as a small supplement to a grid, due to their low power densities and sometimes irregular supply profiles. Hydro-electric power has a relatively large power density and constant power profile, but is entirely dependent on the availability of large bodies of moving water.

Ocean wave energy can compete with traditional sources such a coal and nuclear as it has a high power density in comparison to other renewable sources. Ocean wave energy has a constant power profile and maximum seasonal supply corresponds with the maximum demand. Estimates account for power levels of 1 to 10 TW, available in the world's combined oceans [2]. South Africa is located in a fortunate position, as it has a large coast-line and experiences waves-fronts with an excess of 60 kW per metre wave crest, as shown in Figure 1.1.

Research into extracting energy from ocean waves started in the 1970's [2]. Most traditional devices use waves' mechanical power to pump a hydraulic liquid through a hydraulic motor connected to a rotating generator. This method has two disadvantages: Firstly, the extra energy conversion stages reduce the overall efficiency, and, secondly, the moving mechanical parts require regular maintenance. Maintenance becomes problematic due to the ocean's harsh environment, especially if devices are deployed far off the coast and beneath the water surface.

Linear generators offer a solution to these problems by connecting the translator to a device such as a buoy, which moves with the heaving motion of the waves. This

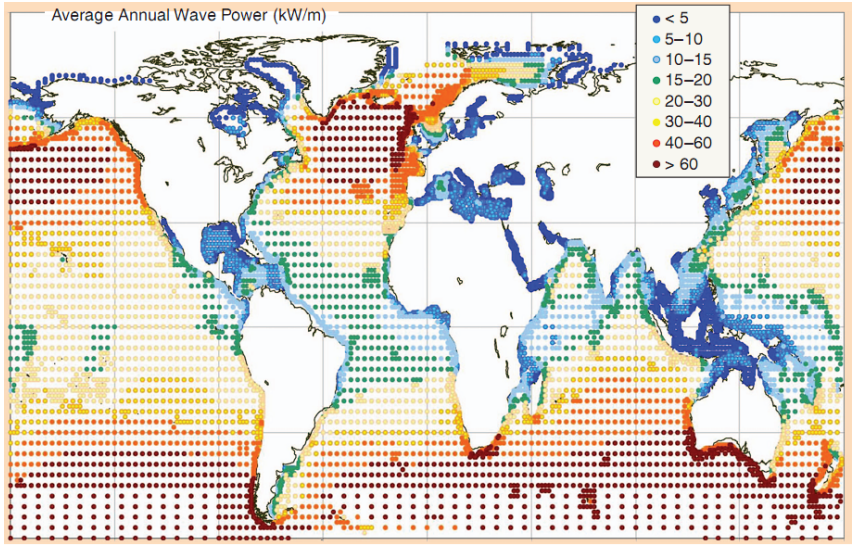

Figure 1.1: Map Showing Annual World Wave Power [1].

direct coupling method eliminates most of the interconnected moving parts, making it a much more robust system. PM linear machines suffer from parasitic forces that cause vibrations and can limit performance and damage the machine. The topic of this thesis is to reduce the cogging forces of a DSTLPMG. This will be achieved by employing Finite Elements Modelling (FEM) to calculate the cogging forces and adjusting the design in an iterative process.

Chapter 2 provides a background into ocean wave energy and the devices used to extract the energy from the waves. Linear generators are briefly discussed as they are used in Wave Energy Converters (WECs).

Chapter 3 introduces the linear machine central to this research. The machine specifications are presented and an initial static force simulation is discussed. Parasitic cogging forces are identified from the simulation results.

Chapter 4 analyses cogging forces present in the static analysis of the linear machine. Cogging forces are explained and different methods of reducing the cogging forces are presented. Results from applying the cogging force reduction methods to the current machine are shown and analysed. The advantages and disadvantages associated with the cogging force reduction methods are discussed.

Chapter 5 summarises the research and presents conclusions drawn from the results. Proposals for future research are presented.

Chapter 2

Background

Introduction: *The ocean contains a vast amount of energy in the form of waves and tides. As we are driven to find alternatives to fossil fuel energy sources ocean wave energy becomes a more interesting option. This chapter briefly explains how ocean waves are formed and some of the existing techniques of how the energy is extracted. Linear generators are discussed as they have application in electricity generation from ocean waves and are central to the topic of this thesis.*

2.1 Ocean Waves

The most common form of ocean waves, called wind waves, are generated by stress applied to the ocean surface by wind [3]. Initially small capillary-waves are formed, which are restored by the surface tension of the water. As more energy is transferred, waves with longer wavelengths and larger wave-heights are formed and are increasingly influenced by gravity, to the extent that it becomes the primary restoring force. Waves which are under the influence of the wind are called sea waves. The area where the wind interacts with the ocean surface is called the fetch box. When the waves have left the fetch box they are called swell waves.

An important point to note is that a wave consists of energy being transported forward,while water particles move in a circular fashion and become more elliptical the closer they get to the ocean floor. This is illustrated in Figure 2.1. Waves are not monochromatic: Spectral components develop with time as energy is transferred from the wind. High frequency components are initially present, but gradually saturate while low frequency components continue to grow. Several energy density wave spectra have been proposed, but the most commonly used model is called the

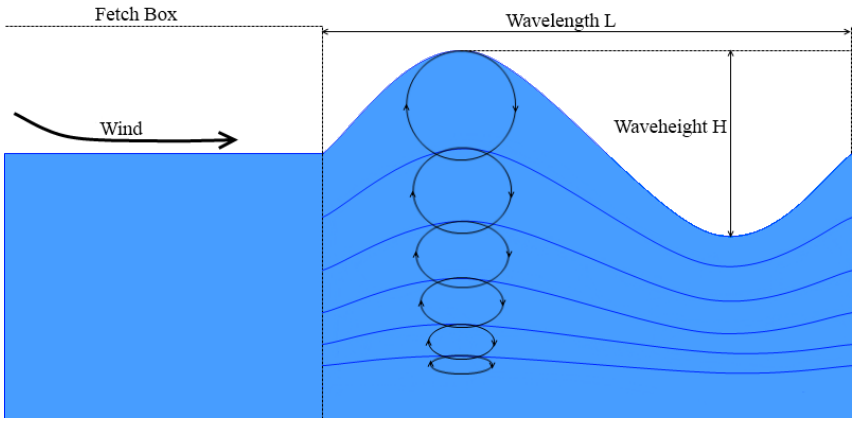

Figure 2.1: Waves are formed by winds imparting energy onto the ocean surface.

Joint North Sea Wave Project (JONSWAP) [3]. JONSWAP describes the energy spectrum of random ocean waves with typical frequencies between 0.04 Hz and 0.25 Hz. This shape is very similar to the Max Plank's curve showing black-body radiation[4]. The position of the spectral peak is dependent on the wind speed in the fetch box and the fetch box length. It is important to take the wave energy spectra into account when designing WECs.

2.2 Wave Energy Converters

The concept of converting ocean wave energy into usable forms has been explored for over two centuries [5]. The earliest patent for this concept was filed in 1799 in France and more than a thousand patents were registered by 1980 [6]. Yoshio Masuda started developing wave powered buoys in the late 1940's. This is seen as the start of modern wave energy technology and has inspired many other devices since. There are many reviews and categorisations of the different types of WECs [5, 7–10]. The author will use the categories created by Falcão [6] as they are very thorough. Not every WEC device and type will be explained in detail except for devices that use linear generators.

Falcão groups all WECs into three main categories, with each main category being

devised into a further two sub categories. The differentiation amongst the main categories is based primarily on the Power Take Off (PTO) mechanism. Sub-categories are differentiated based on the mooring system or the position relative to the ocean surface or shoreline. The following sections describe the three main types of WECs:

2.2.1 Oscillating Water Columns

Oscillating Water Columns (OWCs) consist of a partly submerged chamber with an opening below the water surface. As the water level inside the chamber changes, air is forced in and out of another opening. An air turbine (typically a Wells turbine) is placed in the opening connected to a generator to convert the flowing air into electricity. OWCs can be constructed on the shoreline or off-shore.Off-shore devices are fixed to the seabed or float on the water surface.

2.2.2 Overtopping Devices

Overtopping devices capture water from the wave crest into a reservoir that is positioned higher than the average surrounding water surface. The water is allowed to flow past a hydraulic turbine, converting the potential energy into electrical energy. Some of these devices have parabolic shaped collectors that concentrate the wave energy, thereby increasing the wave height and allowing more water to spill into the reservoir. Similar to OWCs, overtopping devices can be placed on the shoreline or off-shore. Off-shore devices are either fixed or float on the water surface.

2.2.3 Oscillating Bodies

An oscillating body WEC takes advantage of the heaving (linearly vertical) or rotational, reciprocal motion of ocean waves. Unlike OWCs that uses the change in water level, oscillating bodies use the forces on physical bodies interacting with waves against a fixed reference frame. The reference frame can be the ocean floor or another floating object with a much larger inertia. Rotating converters move in a pitch or surge motion. These devices use hydraulic rams or pistons to pump hydraulic fluid through a hydraulic motor connected to a rotating generator.

Oscillating bodies moving in a heaving motion use the linear reciprocal motion of a buoy connected to a hydraulic pumping system or directly to a linear generator. The former method is similar to the rotating converters, while the latter is more interesting as it relates to the topic of this thesis. Directly connected or direct drive systems are more efficient and robust as it removes the intermediate energy conversion stages. The design of the linear generator is critical as the system efficiency is largely dependent on its efficiency.

2.3 Linear Machines

A linear machine converts the mechanical energy of linear motion into electrical energy (or vice versa) without the need for intermediate gears, screws or crank shafts. It can be visualised as a rotating machine cut open along its axis and flattened out. Like its rotating counterpart, linear machines can be based on the following electromagnetic designs:

- Induction Machine
- Synchronous Machine
- Reluctance Machine

All of the above designs can be further classified by a combination the following topologies [11]:

- Flat or Tubular.
- Single Sided or Double Sided.
- Slotted or Slotless.
- Iron-Cored or Air-Cored.
- Transverse Flux or Longitudinal Flux.

A linear machine needs to provide high performance at low speeds and have a simple structure (for high reliability) for it to be acceptable in a WEC [12]. Linear PM synchronous machines are the most suitable under these criteria [13] because:

- It has a high force density.
- It has a reasonable efficiency at low speeds.
- Magnets are becoming less expensive.
- There is no electrical contact between the stator and translator.

Single sided linear machines suffer from a strong attractive normal force between the translator and stator. This force seeks to close the air-gap and exerts huge pressure on the bearings. To eliminate or minimise this force, linear machines are typically designed as a double sided or tubular topology. This results in a zero net force acting on the translator. The reader is directed to [11] and [14] for more in depth theory on PM machines.

The following chapter will discuss a novel linear generator that is a combination of double sided and tubular topologies.

2.4 Conclusion

The majority of ocean waves are generated by winds blowing across the water surface. The wind transfers energy into the water causing oscillations that eventually become waves. These sea waves can travel for large distances with very little energy loss. It is this energy in the waves that humans have been trying to harvest for over two centuries, modern WECs started with Yoshio Masuda's wave powered buoys in the 1940's. Since then many different devices have been created. This chapter follows a categorisation of WECs created by Falcão, the three main categories are: oscillating water columns, overtopping devices and oscillating bodies.

Linear generators are often used in oscillating bodies as the linear reciprocal motion can be directly converted into electricity without the need for gears, screws or crank shafts. Linear generators can be thought of as a rotating generator cut open along its axis and flattened out. Linear generators are ideal for use in WECs, but need to provide high performance at low speeds and have a high reliability. The next chapter discusses a new linear generator design that addresses these issues.

Chapter 3

Double Sided Tubular Linear Permanent Magnet Generator

Introduction: *Linear machines are available in differing topologies, each with inherent advantages and disadvantages. A linear generator's force capability is directly proportional to the amount of magnetic flux linking the stator and translator. This, in turn, is dependent on the air-gap surface area. An increase in air-gap surface area translates into a directly proportional increase in machine cross section for flat and tubular layouts. This becomes problematic for the use of linear machines in WECs as large machines are costly to transport and maintain. The design of a novel linear generator to overcome this limitation will be discussed in this chapter.*

3.1 Machine Description

The University of the Witwatersrand set out to design a WEC that would have a higher power density, resulting in a lower spatial footprint and ultimately a lower cost. This machine, proposed and designed by D. Joseph[15], combines the increased force capability of a double-sided flat layout with the ability to encapsulate/contain the magnetic field from a tubular layout. The resulting design is called a DSTLPMG. The DSTLPMG has a lower volumetric footprint for the same force capability when compared to a similar double-sided flat layout [4].

The machine consists of two tubular stators with a translator sandwiched in between (Figure 3.1). A 5 kN prototype has been built for static force testing. The machine properties are listed in Table 3.1. To assess its performance, simulations of the prototype design have been concluded in two different FEM packages, ANSYS and

COMSOL. The total axial force acting on the translator was calculated and recorded for each incremental displacement step across one pole pitch. The radial force was neglected as the radial forces cancel because of the tubular nature of the design.

The stator is slotted to increase the force density of the machine, the downside to this design is that the magnets will interact with the stator slots and create a ripple in thrust force called slot cogging.

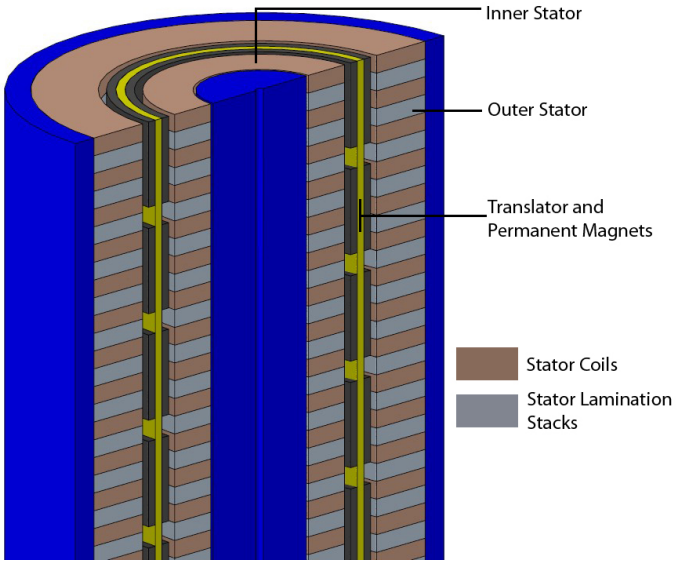

Figure 3.1: Cut-Out of the DSTLPMG.

The simulation results (Figure 3.2) show that the force is composed of multiple components each with different periods and amplitudes. These "parasitic" components are called cogging forces and are detrimental to the operation of the machine. The cogging forces will be discussed in the next chapter.

3.2 Conclusion

This chapter introduces a novel linear machine for ocean wave energy conversion called a DSTLPMG. The machine is a combination of a flat and tubular topology, this increases the air-gap size without a proportional increase in size and encapsulates the magnetic flux for an increased force density. Static force simulations were done on a model based on a physical prototype, the simulation results showed significant cogging forces that will have a negative effect on the machine operation. The cogging forces are discussed in the next chapter.

Table 3.1: Prototype Specifications.

Property Name	Value
Stator Length	0.365 m
Translator Length	1.00 m
Pole Pitch	0.06 m
Magnet Pitch	0.048 m
Translator Inner Radius	0.073 m
Translator Outer Radius	0.078 m
Slots/Pole/Phase	1
Magnet Thickness	5.0 mm
Air-gap Length	4.5 mm
Conductor Current Density	5 A/mm^2

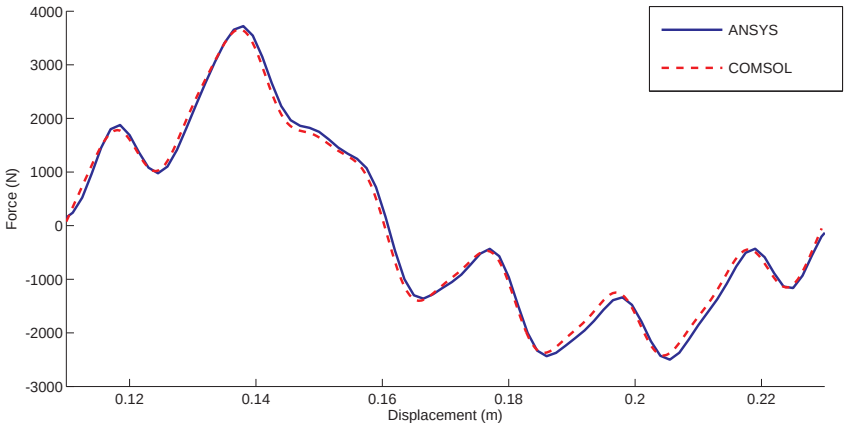

Figure 3.2: Translator Force Simulation Done in ANSYS and COMSOL.

Chapter 4

Cogging Force.

Introduction: *Cogging forces arise from the attraction between the PMs and the armature core [16]. The magnet array attempts to align itself in a position that results in the minimum magnetic energy when the system is unexcited [17]. Cogging causes mechanical vibrations that can damage the stator teeth and the PMs [18], as well as destroy the airgap [19]. Due to the fluctuations in velocity, cogging also produces output power fluctuations. The total cogging force can be divided into two forces created by different mechanisms: slot cogging and end-effect cogging. Slot cogging is a common problem amongst rotating machines, while end-effect cogging is unique to linear machines [20]. Figure 4.2 illustrates the difference between slot and end-effect cogging. Slot cogging is caused by the interaction between the PMs and the armature slots and usually has a period of one slot pitch. End-effect cogging, however, is caused by the interaction between the PMs and the stator ends and has a period of one pole pitch.*

A note on axisymmetry: The simulations were done using an axisymmetric model. This allows for models that are symmetrical about an axis to be modelled in 2D, but the calculations are performed in 3D by rotating the 2D model around the axis of symmetry. The coordinate system is identified by r and Z and the axis of symmetry is $Z = 0$.

This chapter identifies the cogging forces in the DSTLPMG translator force and discusses methods of reducing it. Figure 4.1 shows the harmonic content of the translator force from Figure 3.2. It is immediately apparent that the cogging forces are significant compared to the thrust force (fundamental). The sizes of the second and sixth harmonics are 29 % and 22 % of the thrust force respectively. The second and fourth harmonics are all part of the end-effect cogging force and the sixth

harmonic is the slot cogging force.

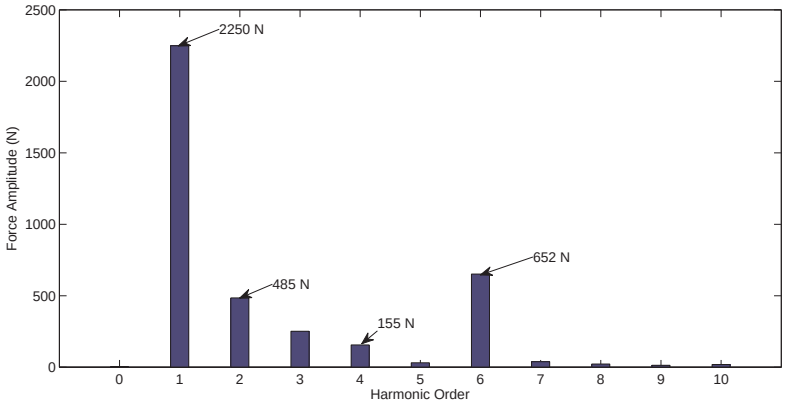

Figure 4.1: Harmonic Content of Total Force.

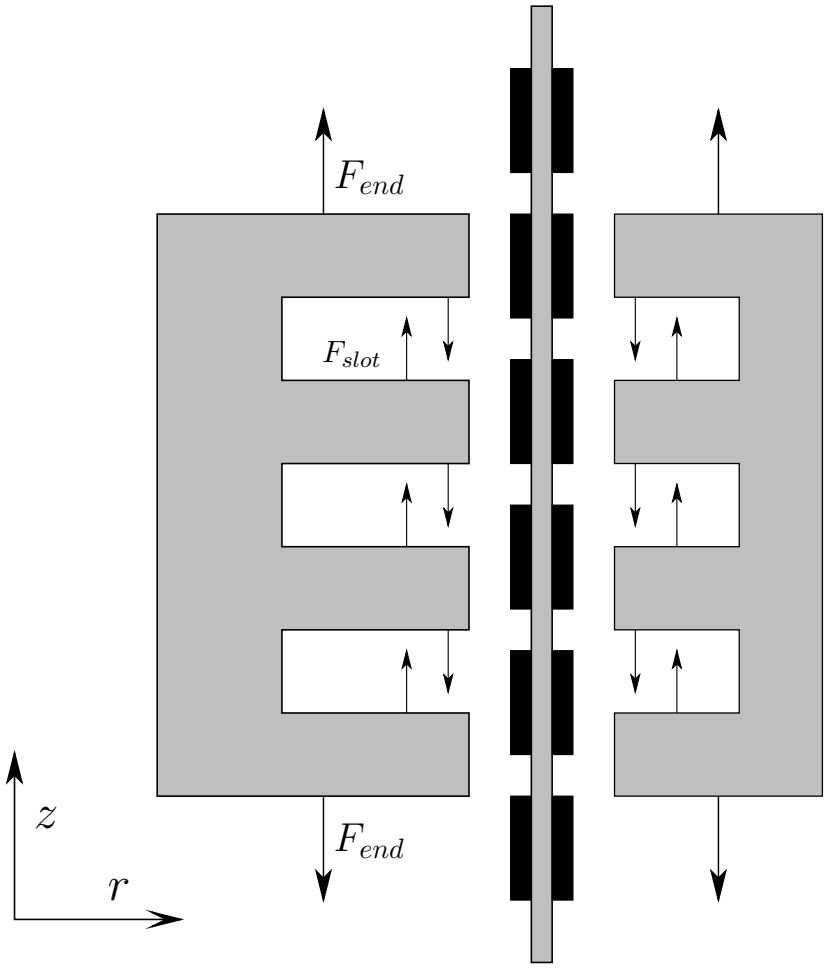

Figure 4.2: Cogging Forces.

4.1 End-Effect Cogging Forces

4.1.1 Description

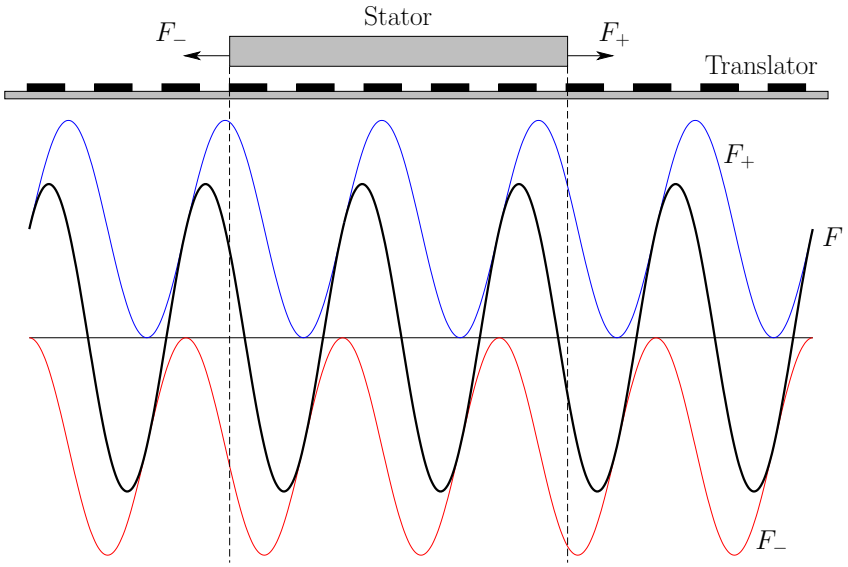

Figure 4.3: Total Cogging force Comprising of Two End Forces

The total end-effect cogging force comprises of two normal forces acting on each stator end. Each force is unidirectional and acts in opposite directions [21]. Consider the basic linear machine in Figure 4.3, F (thick curve) is given by:

$$F = F_- + F_+ \tag{4.1}$$

The relationship between F_- and F_+ is given by [21]:

$$F_-|_{z=z'} = F_+|_{z=-(z'+\delta)} \tag{4.2}$$

δ is defined as:

$$\delta = L_s - k\tau \qquad k \in \mathbb{Z} \tag{4.3}$$

The amplitude is dependent on the phase shift between F_- and F_+, which in turn is dependent on the stator length [22]. Therefore, F can be minimized by choosing an appropriate stator length.

The required phase shift can be derived by expressing each force as a generalized Fourier Series and noting the relationship in Equation 4.2.

$$F_+ = F_0 + \sum_{n=1}^{\infty} F_{sn} \sin(\frac{2\pi n}{\tau} z) + \sum_{n=1}^{\infty} F_{cn} \cos(\frac{2\pi n}{\tau} z) \tag{4.4}$$

According to Equation 4.2, F_- can be written as:

$$F_- = -F_0 + \sum_{n=1}^{\infty} F_{sn} \sin(\frac{2\pi n}{\tau}(z+\delta)) - \sum_{n=1}^{\infty} F_{cn} \cos(\frac{2\pi n}{\tau}(z+\delta)) \tag{4.5}$$

By Equation 4.1:

$$\begin{aligned} F &= F_- + F_+ \\ &= \sum_{n=1}^{\infty} F_{sn} \sin(\frac{2\pi n}{\tau} z) + \sum_{n=1}^{\infty} F_{cn} \cos(\frac{2\pi n}{\tau} z) \\ &\quad + \sum_{n=1}^{\infty} F_{sn} \sin(\frac{2\pi n}{\tau}(z+\delta)) - \sum_{n=1}^{\infty} F_{cn} \cos(\frac{2\pi n}{\tau}(z+\delta)) \\ &= \sum_{n=1}^{\infty} 2[F_{sn} \cos(\frac{n\pi}{\tau}\delta) + F_{cn} \sin(\frac{n\pi}{\tau}\delta)] \sin(\frac{2\pi n}{\tau}(z+\delta/2)) \end{aligned} \tag{4.6}$$

The full derivation can be seen in Equation A.1 found in Appendix A. The optimum stator length can be found by setting Equation 4.6 to zero and solving for δ, this gives:

$$\delta = \frac{\tau}{n\pi} \arctan(-\frac{F_{sn}}{F_{cn}}) \tag{4.7}$$

The value of δ is the difference between the optimum stator length and the nearest integer multiple of pole pitches. Any harmonic in the total force can be eliminated by choosing an appropriate value for n. $N = 1$ would eliminate the fundamental component. In practice the magnetic and geometric lengths of the stator differ [22], therefore manually calculating the phase difference between the top and bottom forces yield more accurate results.

4.1.2 Reduction

In order to reduce the end effect cogging forces, a FEM simulation of the original machine was performed with no slots and no excitation. This removes the contribution of the slot cogging and thrust forces. Forces were calculated using a local application of the Maxwell Stress Tensor Method. By integrating over specific surface areas, the forces acting on the top and bottom faces could be isolated. The stator was moved over a distance of two pole pitches in increments of $\frac{2\tau}{255}$. The end-effect cogging forces for the original machine are given in Figure 4.4 and the harmonic content of the total force is shown in Figure 4.5.

The top and bottom forces contain significant 2'nd harmonic components which distorts the shape. This makes it impossible to eliminate the total cogging force by changing the phase shift. It can be minimised, however, by eliminating the largest harmonic which is the fundamental. This is done by calculating the phase shift between the fundamentals of the top and bottom forces and adjusting the stator length by that amount. This process is iterative and often requires small adjustments to align the fundamentals entirely.

The initial phase shift was 3.67 cm, requiring the stator length be adjusted to 0.3967 m. The length required further adjustments. The final length was 0.3948 m. In comparison, when using Equation 4.7 and 4.3, L_s is 0.4104 m for $k = 7$. This reveals a 3.3 % difference between the calculated and simulated values. Figure 4.6 shows the results after the adjustments.The peak cogging force has been reduced by 63 % from 630 N to 233 N. The total cogging force, however, still retains a significant second harmonic.

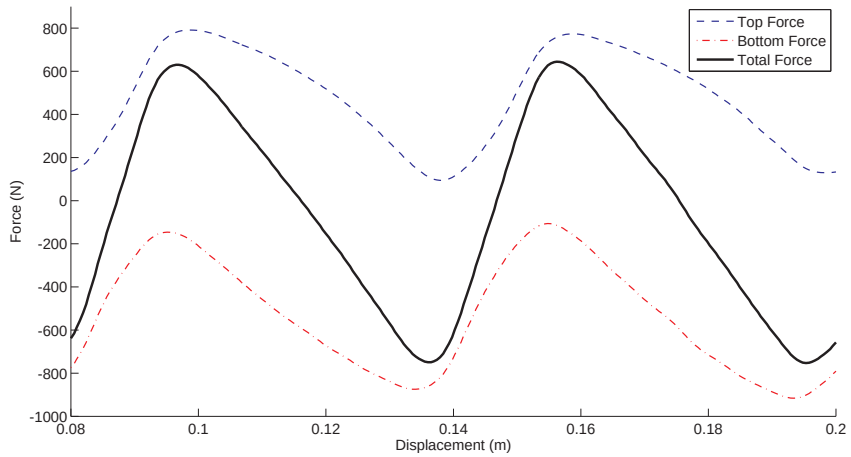

Figure 4.4: End Effects Cogging Force of the Original Machine.

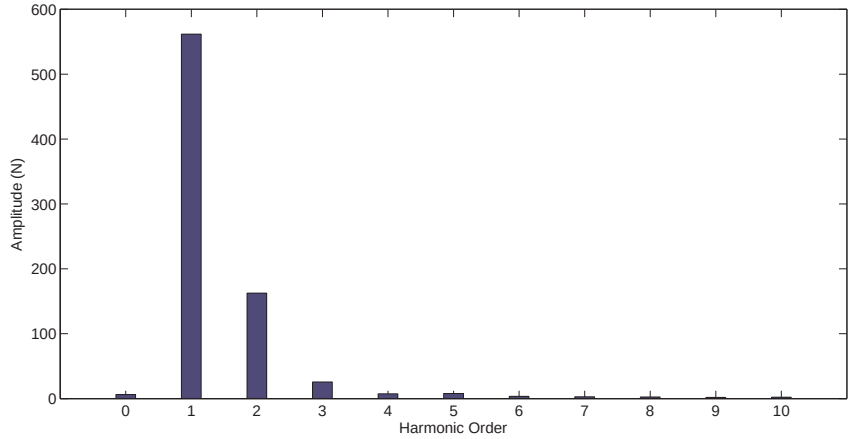

Figure 4.5: Harmonic Content of the Total Force.

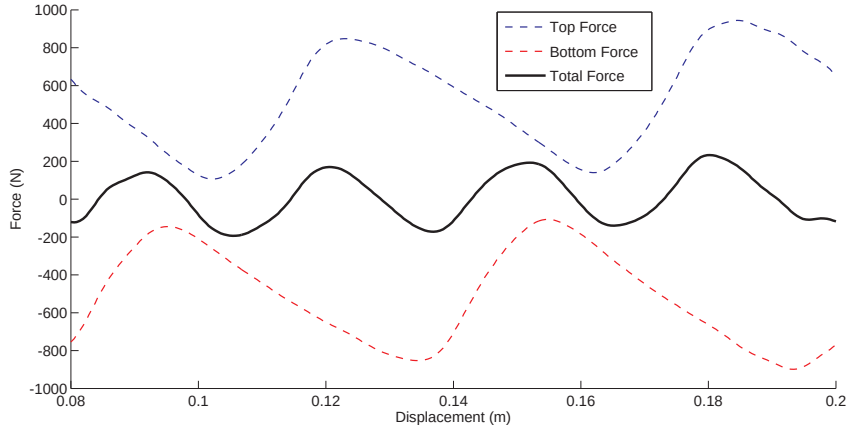

Figure 4.6: End Effects Cogging Force with Cancelled Fundamentals.

4.1.3 Stator Ends Shaping

Triangular Shape

Wang et.al. [23] have suggested reducing the second harmonic component by altering the shape of the stator ends. Diagram Figure 4.7 shows that the stator ends are skewed by half a pole pitch in the Φ direction. The faces are skewed symmetrically to avoid any unbalanced radial forces. Assuming that the total force acting on a face is the average of the axial forces acting on an infinite number of iron particles with axial displacement z, the total force acting on the top face can be described as:

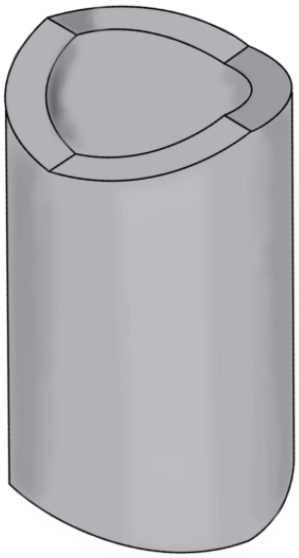

Figure 4.7: Stator with Skewed Ends.

$$\begin{aligned} F_{top\_sk}(z_d) &= \frac{2}{\tau}\int_{z_d-\frac{\tau}{4}}^{z_d-\frac{\tau}{4}} F_+(z)dz \\ &= F_0 + \sum_{n=1}\frac{2}{n\pi}\sin(\frac{n\pi}{2})[F_{sn}\sin(\frac{2\pi n}{\tau}z_d) + F_{cn}\cos(\frac{2\pi n}{\tau}z_d)] \end{aligned} \tag{4.8}$$

Two important effects of the skewing can be seen in Equation 4.8:

1 For n even, $\sin(\frac{n\pi}{2}) = 0$

2 The magnitude of other harmonics is reduced by a factor of $\frac{2}{n\pi}$

The same method can be applied to the bottom face. Using this technique, the second harmonic can be eliminated. However, this method cannot be simulated, and thus verified, using an axisymmetric model. This method was modified so that it could be simulated using an axisymmetric model by applying the skew in the radial direction. A linear slope was created from the inner to the outer radii in order for the resulting faces to look triangular from an axisymmetric perspective. This is illustrated in Figure 4.8.

Figure 4.9 shows the harmonic content of the top stator end force for the original and the triangular stator ends. The triangular shape does not have the desired effect

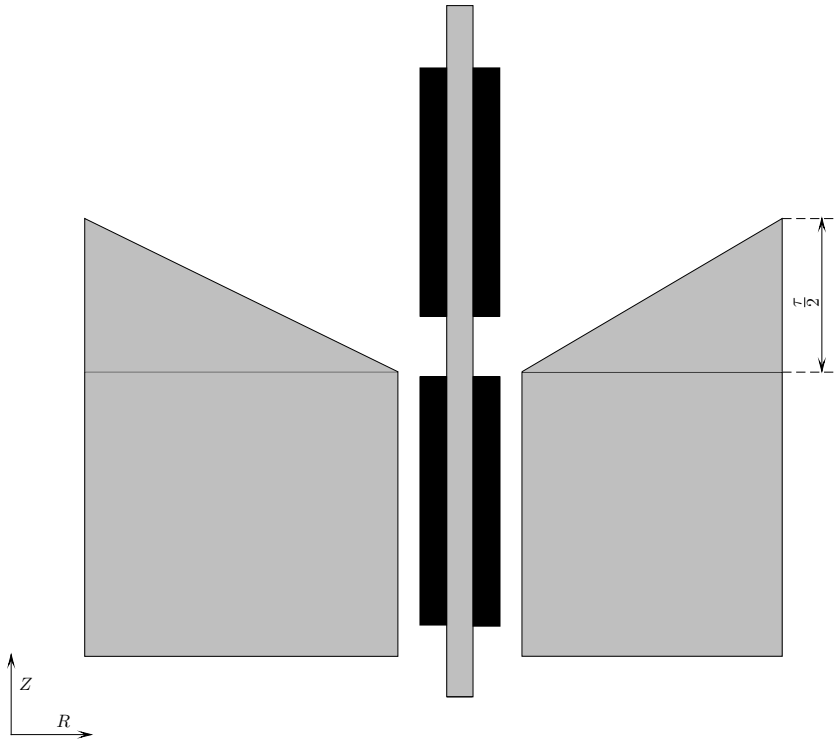

Figure 4.8: Triangular Stator End Shape.

on the cogging force as it leads to an increase in cogging force. This can be explained by noting that the integral in Equation 4.8 only holds if the total flux tube falls on the entire face of the stator end, resulting in the force being integrated over a height of $\frac{\tau}{2}$. Figure 4.10 shows that this is not always the case, as the flux is more inclined to flow through the closest section of the face. The top face area is larger than in the original flat top face, due to the hypotenuse of a right angled triangle being the largest side. This allows more flux to flow through the face, resulting in a larger force.

By dividing the stator end face into a sloped and flat section, the majority of the flux can be guided to flow through the sloped section spanning a height of $\frac{\tau}{2}$. This is illustrated in Figure 4.11. The ratio between r_1 and r_2 is defined as $er = \frac{r_2}{r_1+r_2}$, the value er was varied between 0 and 1 in steps of 0.05 while the top force and harmonics were calculated. A plot of the fundamental, second and third harmonics vs. er is shown in Figure 4.12. Not all three curves reach a minimum at the same value of er. The point where the second harmonic reaches a minimum is the most important, as the fundamental can be eliminated by resizing the stator. The second harmonic does not entirely reach zero, however the minimum value happens at $er = 0.9$. The fundamental was minimised by using the above approach to resize the stator. Figure

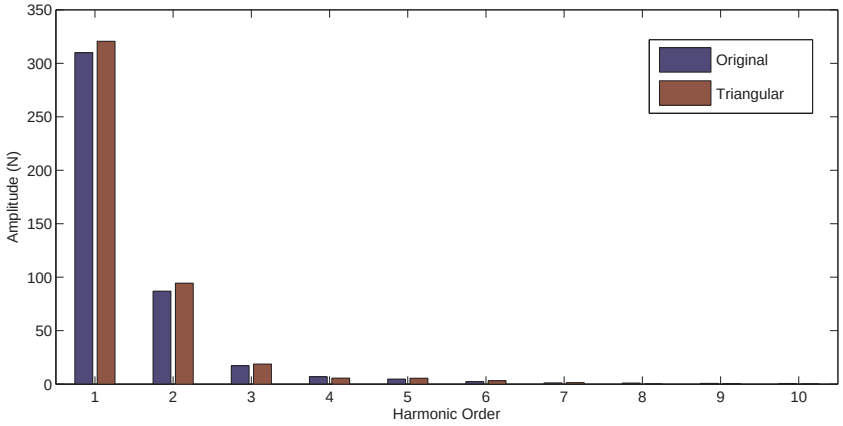

Figure 4.9: Harmonic Content of Original Stator Ends vs. Triangular Ends.

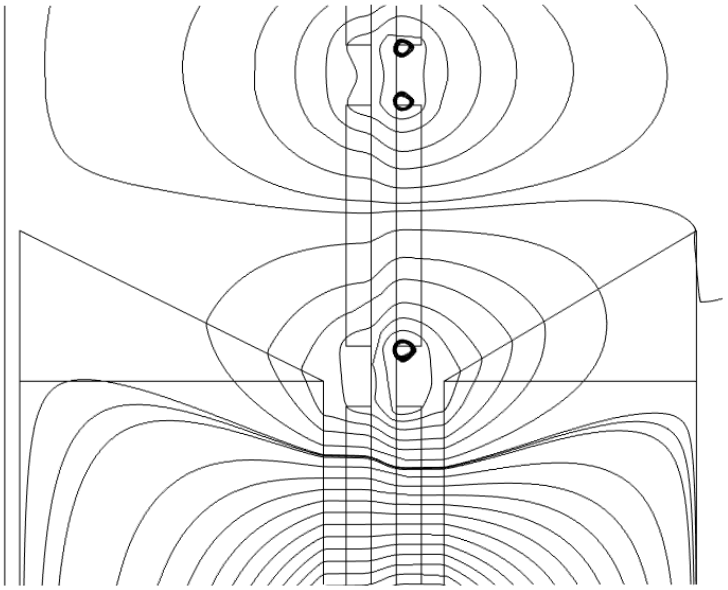

Figure 4.10: Flux Lines at the Top Stator Ends.

4.13 shows the top and bottom cogging forces with each fundamental and the total cogging force. The end effect cogging force was reduced to a peak value of 61 N.

Bézier Curve

An alternative to a triangular shape is a Bézier curve. A Bézier curve is a parametric curve defined by control points and the weights of each control point [24]. For n control points the resulting shape would be a polynomial of order $n - 1$. Stator end-faces with a quadratic curve shape were created and are shown in Figure 4.14.

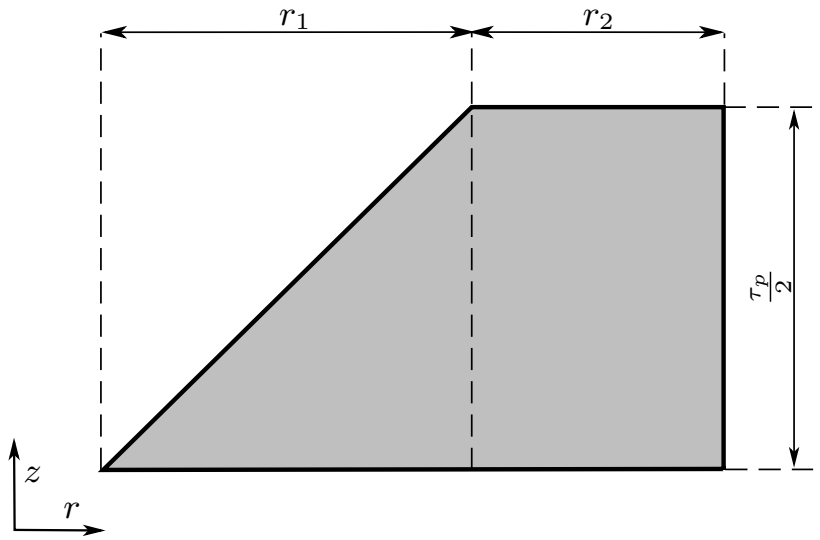

Figure 4.11: Outer Stator Top Face with Two Sections.

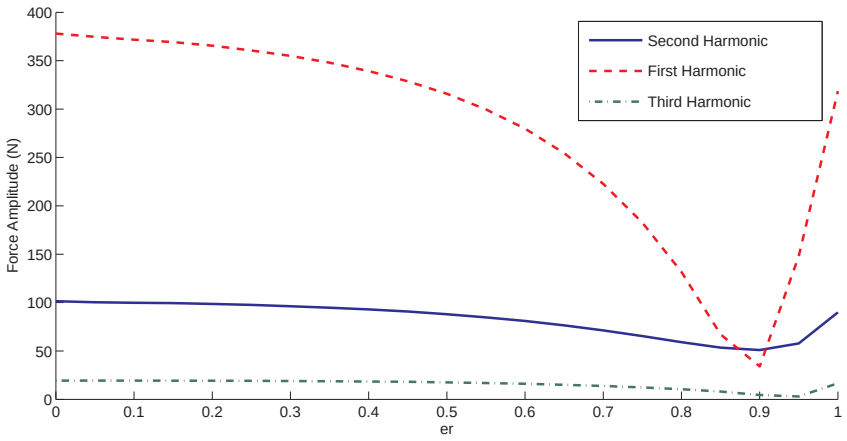

Figure 4.12: Harmonic Amplitude vs. er.

The control points (P_0, P_1, P_2) are positioned on three corners of a rectangle with a width of the stator and a height of half a pole pitch. The weights are left as the default COMSOL values (1, $\frac{1}{\sqrt{2}}$ and 1). The top force was calculated for a distance of 2 pole pitches, while the harmonics were calculated and are compared to the original top values in Figure 4.15. The second harmonic was reduced from 310 N to 230 N. This is a substantial improvement, but not significant enough to justify using the method.

The stator ends were divided into two sections, which bear similarity to the triangular shape (shown in Figure 4.16). The ratio between the radial lengths of the two sections is defined as $er = \frac{r_2}{r_1+r_2}$. The top cogging force was calculated over two

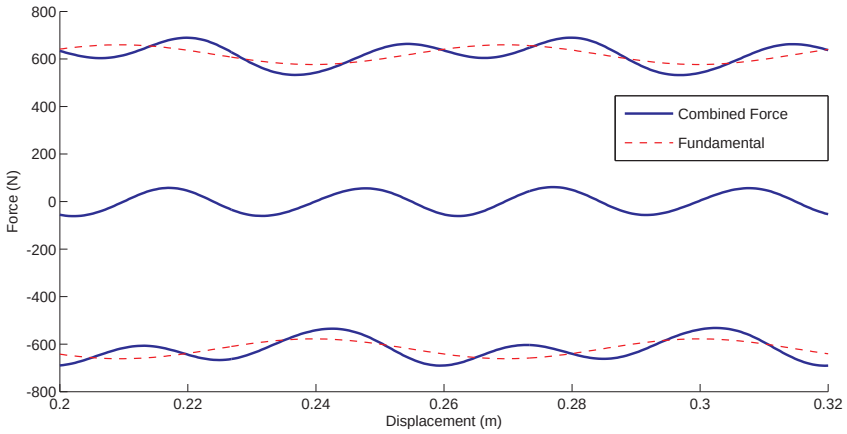

Figure 4.13: Top, Bottom and Total Cogging Forces with Optimised Triangular Shape and Stator Length.

pole pitches for values of er between 0 and 1 in steps of 0.05. Figure 4.19 shows the amplitude of the fundamental, first and second harmonics in regards to er. The second harmonic is at a minimum at $er = 0.8$. Figure 4.17 shows the shape of the cogging forces with the altered stator end shape. Figure 4.18 shows the cogging forces after the stator length has been optimized, resulting in the total cogging force being reduced to a peak of 7 N.

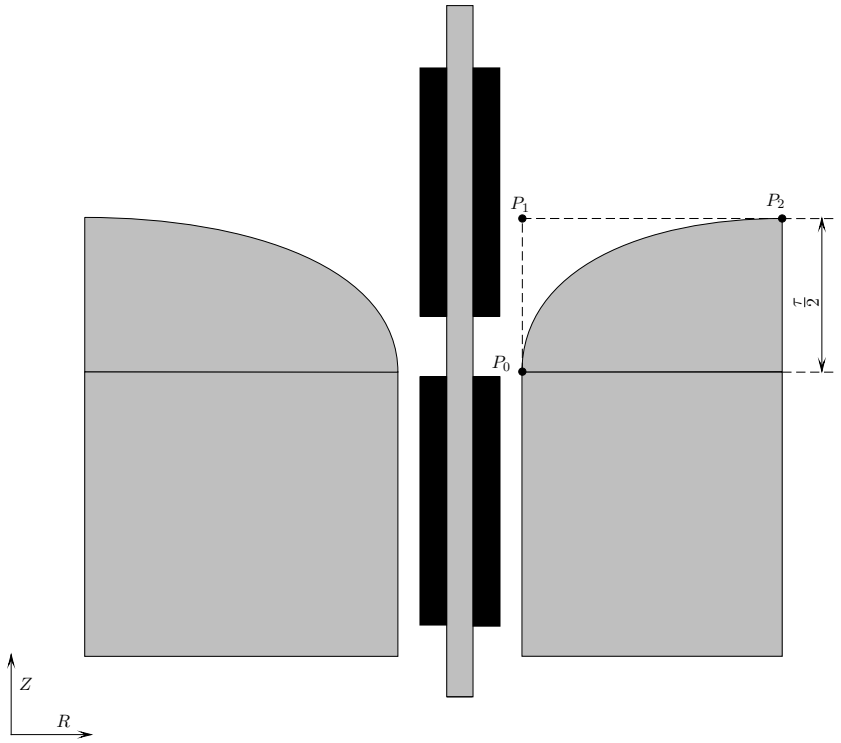

Figure 4.14: Inner and Outer Top Stator Ends.

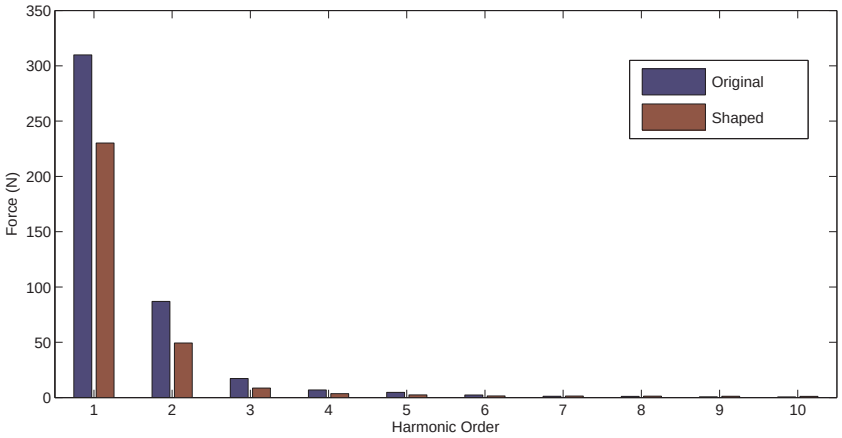

Figure 4.15: Harmonic Content of Original Stator Ends vs. Shaped Ends.

Stepped Rectangular Shape

Considering that a complex shape such as the one presented above would likely pose manufacturing difficulty, an alternative method of reducing the second harmonic is necessary. This can be solved by creating a stepped face with a step height of $\frac{\tau}{4}$ as shown by Wang [23]. If the two faces have equal areas the top force can be expressed as:

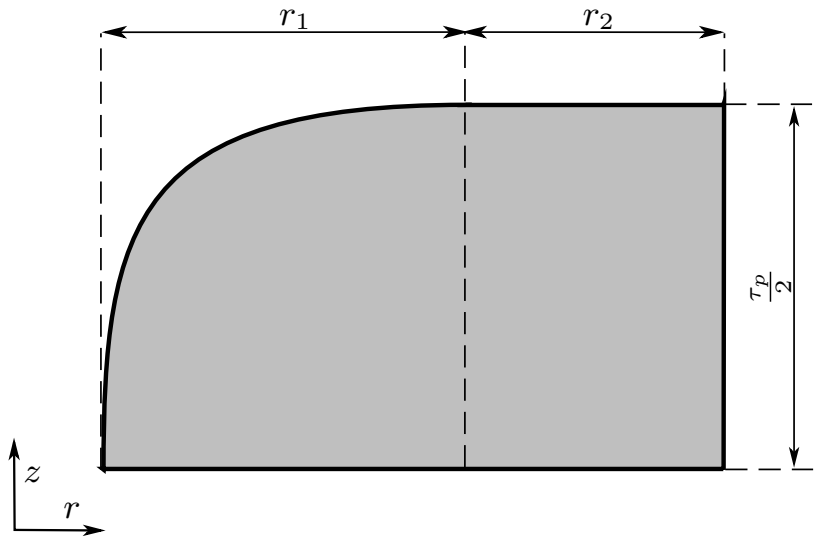

Figure 4.16: Shaped Stator End Broken Up Into Two Sections.

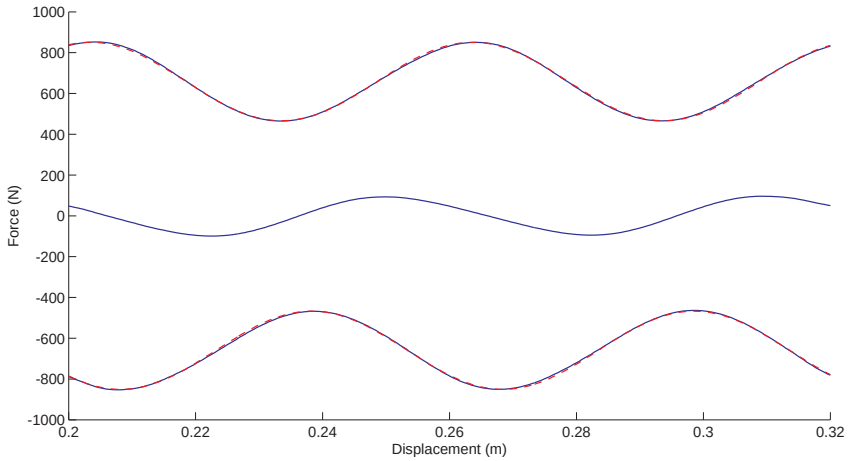

Figure 4.17: End Effects Cogging Force with the Optimised End.

$$
\begin{aligned}
F_{top\_step}(z_d) &= F_0 + \frac{1}{2}\sum_{n=1}[F_{sn}\sin(\frac{2\pi n}{\tau}z_d - \frac{\pi n}{4}) + F_{cs}\cos(\frac{2\pi n}{\tau}z_d - \frac{\pi n}{4})] \\
&+ \frac{1}{2}\sum_{n=1}[F_{sn}\sin(\frac{2\pi n}{\tau}z_d + \frac{\pi n}{4}) + F_{cs}\cos(\frac{2\pi n}{\tau}z_d + \frac{\pi n}{4})] \\
&= F_0 + \frac{1}{2}\sum_{n=1}F_{sn}[\sin(\frac{2\pi n}{\tau}z_d - \frac{\pi n}{4}) + \sin(\frac{2\pi n}{\tau}z_d + \frac{\pi n}{4})] \\
&+ \frac{1}{2}\sum_{n=1}F_{cs}[\cos(\frac{2\pi n}{\tau}z_d - \frac{\pi n}{4}) + \cos(\frac{2\pi n}{\tau}z_d + \frac{\pi n}{4})] \\
&= F_0 + \sum_{n=1}\cos(\frac{\pi n}{4})[F_{sn}\sin(\frac{2\pi n}{\tau}z_d) + F_{cn}\cos(\frac{2\pi n}{\tau}z_d)]
\end{aligned}
\tag{4.9}
$$

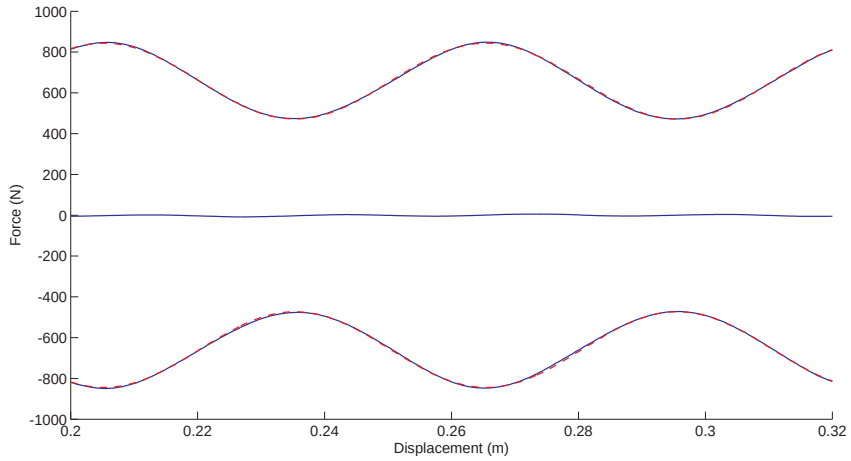

Figure 4.18: End Effects Cogging Force with the Optimised End and Length.

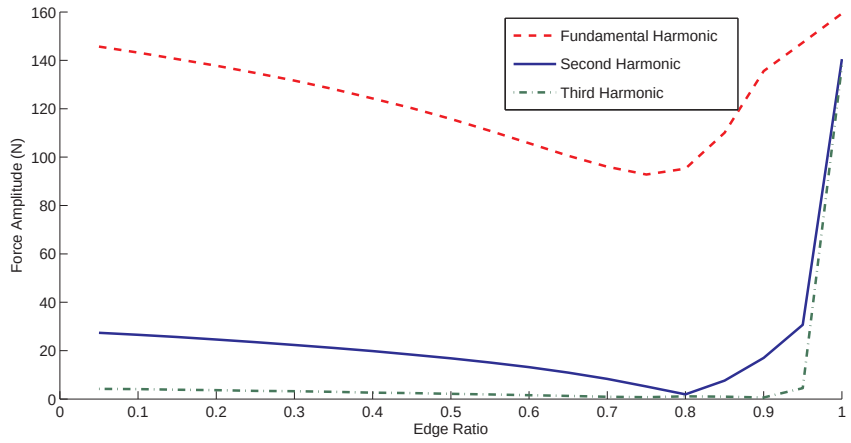

Figure 4.19: Amplitude of Harmonics vs. Edge Ratio.

From Equation 4.9 we can deduce that for $n = 2, 6, 10, ...,$ $\cos(\frac{\pi n}{4}) = 0$.

Unfortunately, however, this method relies on the fact that the steps are in the axial direction. This method cannot be simulated in a 2D axisymmetric simulation. It can, never the less, be modified by stepping the stator-end face in the radial direction and changing the sizes of the end-areas to compensate for the non-uniform flux distribution. The area of the inner stator-end is larger than that of the outer stator, thus making it necessary to only step one of the ends and adjust the radius of the stepped area. A step of height $\frac{\tau}{4}$ was placed on the inner stator end and the radial width was adjusted by reducing the inner and outer radii separately. Two separate configurations were created and tested (Figure 4.20 and Figure 4.21). The ratio $er = \frac{r_2}{r_1+r_2}$ varied between 0 and 1 in steps of 0.05, while the end forces and harmonics were calculated. The fundamental, first and second harmonics were calculated for each value of er, as shown in Figure 4.22 and Figure 4.25. The optimal

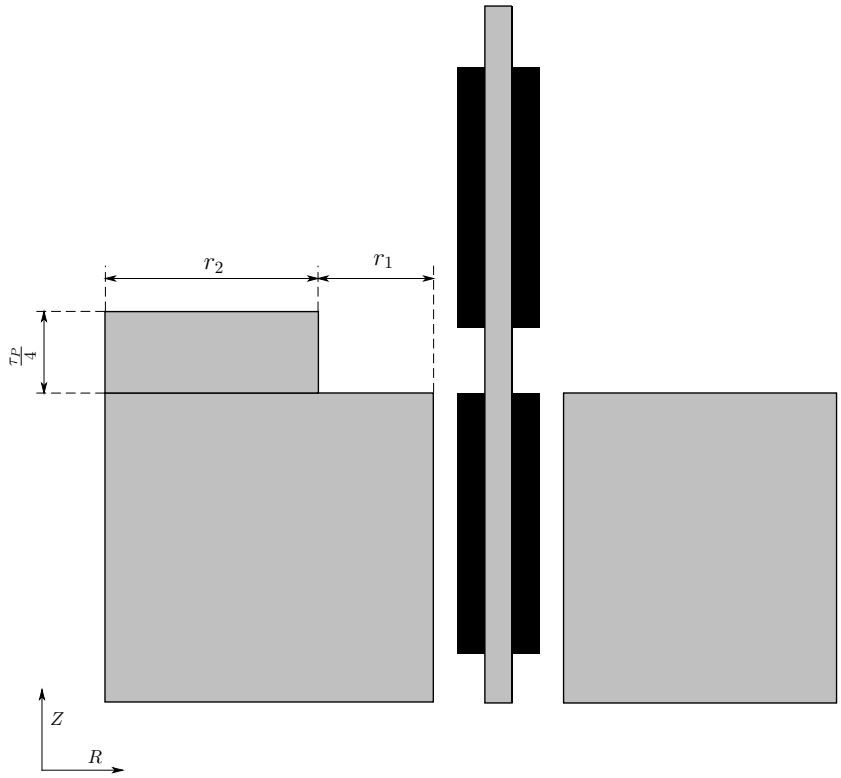

Figure 4.20: Longer Inner Stator Configuration 1

ratio is 1 for configuration 1 and 0.35 for configuration 2. The top, bottom and total cogging forces are shown in Figure 4.23 and Figure 4.26.

Figure 4.22 and Figure 4.25 have similar shaped graphs for the second harmonics. The reason for this is that in configuration 1 the flux falls on the lower surface for most of the values of er, hence the stepped face has no effect. For values $er \geq 0.8$ the stepped face becomes large and close enough for flux to flow through it, as a result the second harmonic becomes increasingly reduced until $er = 1$ where all the flux falls on the stepped edge. Configuration 2 has the opposite effect, for values $er \leq 0.1$ the stepped face is too narrow and not enough flux flows through it for it to make a difference. When er becomes larger the forces on the stepped face become dominant and the change in effect becomes negligible. Even though the minimal amplitude for the second harmonic is at $er = 0.35$, the amplitude of the second harmonic is very similar at $er = 1$. Thus, extending the entire inner stator length by $\frac{\tau}{4}$ shows a significant reduction in the second harmonic.

The stator length was optimized to remove the fundamental harmonic, with the result shown in Figure 4.28.

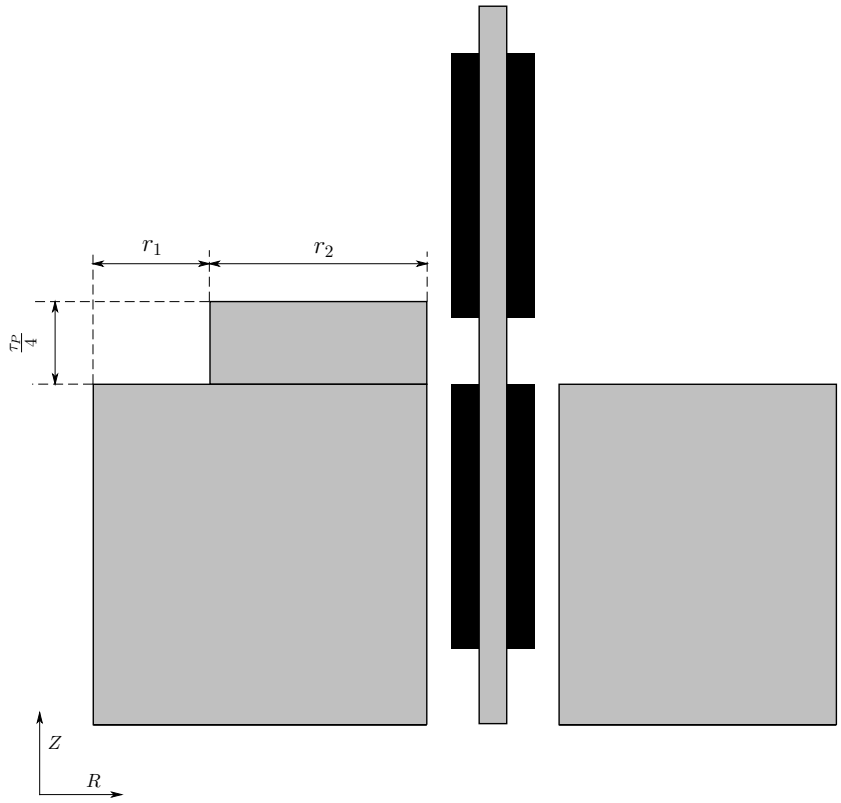

Figure 4.21: Longer Inner Stator Configuration 2

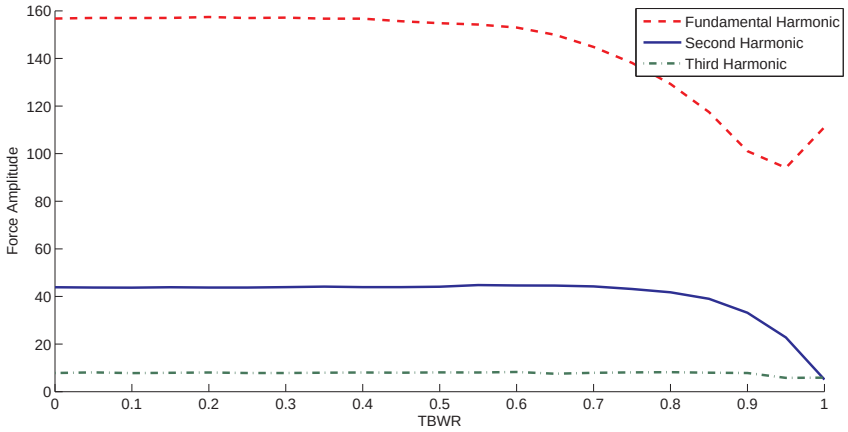

Figure 4.22: Second order harmonic while changing er. (Configuration 1)

4.2 Slot Cogging

4.2.1 Description

The thrust ripples produced by slot cogging is a common problem in rotating PM machines [25, 26]. Slot cogging forces are created by the interaction of the PMs and

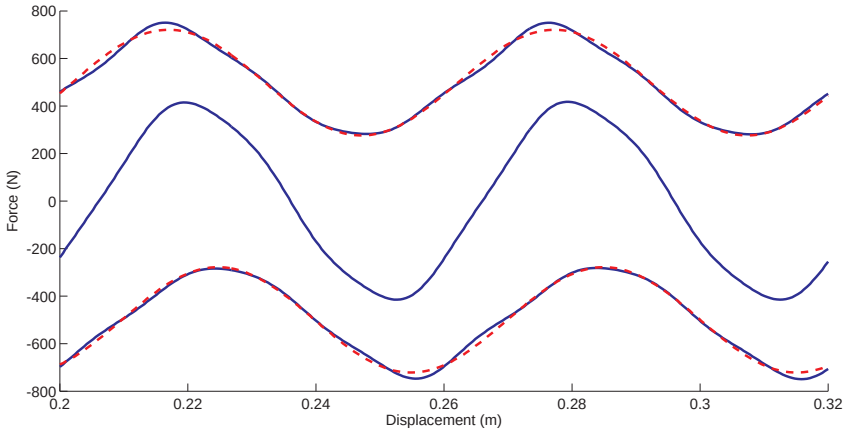

Figure 4.23: Top, Bottom and Total Forces with Optimal End.

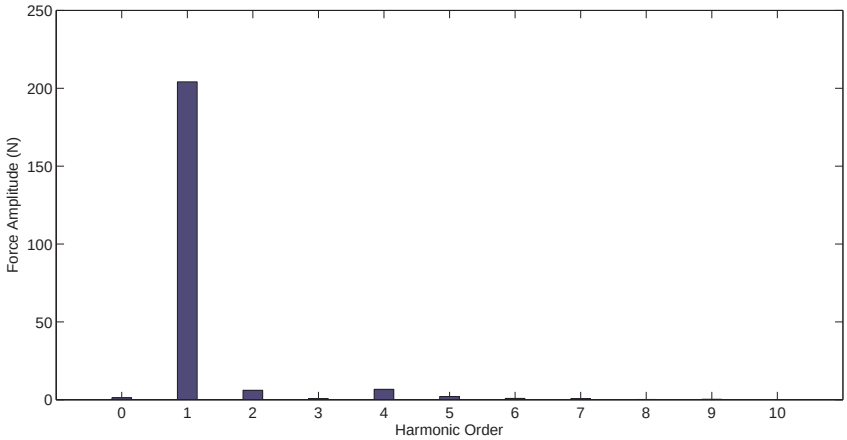

Figure 4.24: Harmonic Content of the Total Force with an Optimal End.

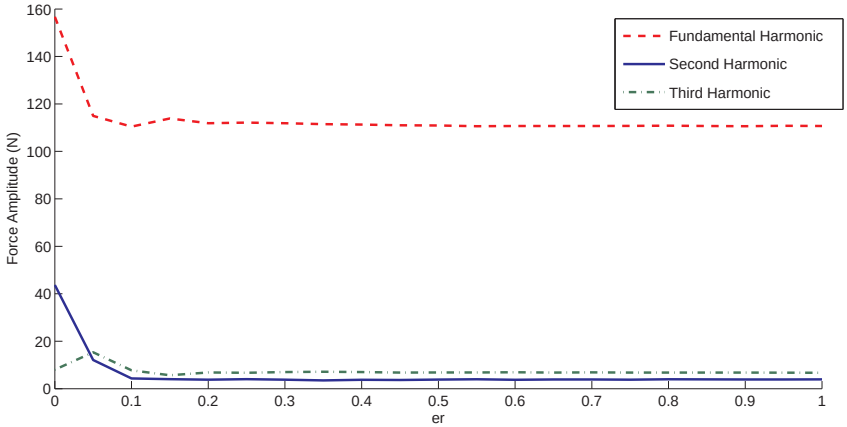

Figure 4.25: Second order harmonic while changing er. (Configuration 2)

the stator slots. The total force is a combination of the cogging force for each stator slot. The following sections will present methods for reducing the slot cogging force.

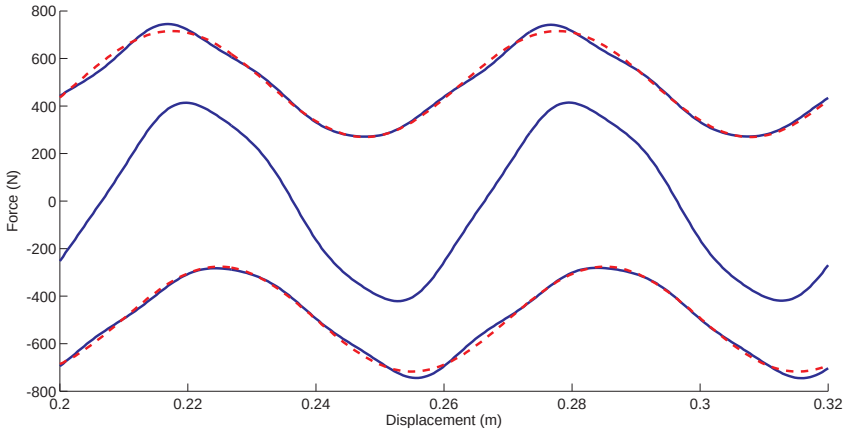

Figure 4.26: Top, Bottom and Total Forces with Optimal End.

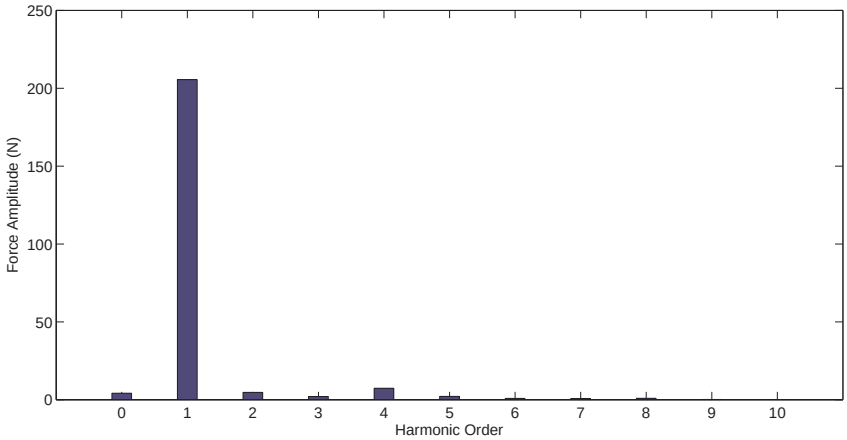

Figure 4.27: Harmonic Content of the Total Force with an Optimal End.

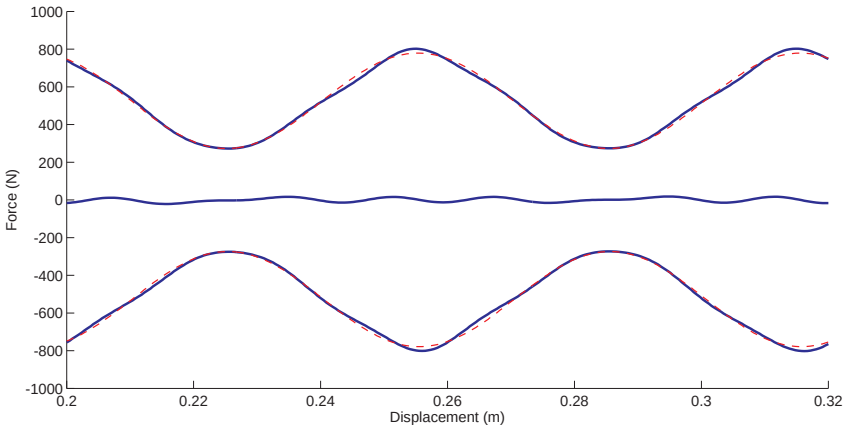

Figure 4.28: Top, Bottom and Total Force with Longer Inner Stator and Optimised Stator Length.

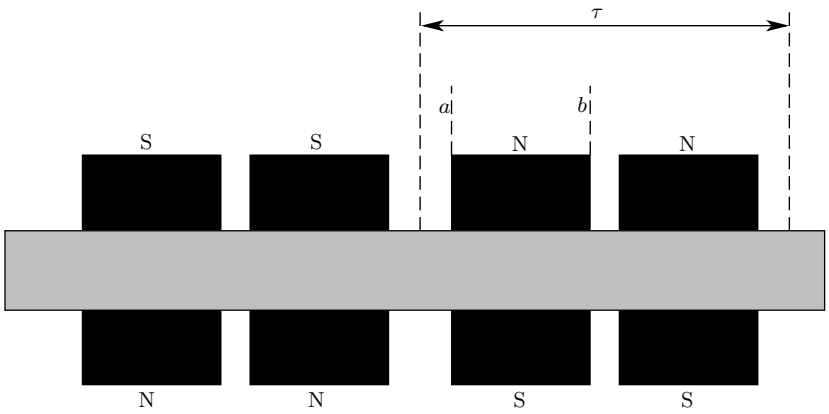

Figure 4.29: Arrangement of divided PMs.

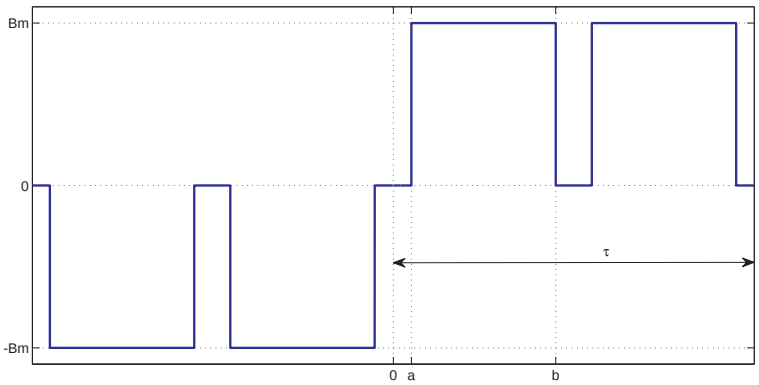

Figure 4.30: Flux Distribution of Divided Magnets.

4.2.2 Magnet Division

The slot cogging force is dependent on the shape of the flux density in the air-gap. A more sinusoidal shape would result in a smaller slot cogging force. Kim et al. proposed reducing removing certain harmonics in the PM flux distribution by resizing and dividing the magnets [27]. By starting with full-sized magnets (the current magnets' width are 80 % of a pole pitch) and assuming a square wave flux distribution in the air-gap, the waveform can be described by a Fourier Series. As considered in Figure 4.29, the magnet geometry is defined by two variables, a and b, and the pole pitch τ. The ideal flux distribution, shown in Figure 4.30, can be

described as:

$$B(\theta) = \begin{cases} B_m & (a \leq \theta \leq b, \tau - b \leq \theta \leq \tau - a) \\ 0 & (otherwise) \end{cases} \tag{4.10}$$

The generalised Fourier series can be expressed as:

$$B(\theta) = B_0 + \sum_{n=1}^{\infty} B_{sn} \sin(\frac{\pi n}{\tau}\theta) + \sum_{n=1}^{\infty} B_{cn} \cos(\frac{\pi n}{\tau}\theta) \tag{4.11}$$

The function given in Equation 4.10 is odd, so B_0 and B_{cn} become zero for all values of n. B_{sn} can be found with:

$$\begin{aligned} B_{sn} &= \frac{4}{T} + \int_0^{\frac{T}{2}} B(\theta) \sin(n\frac{\pi}{\tau}) d\theta \\ &= \frac{2B_m}{n\pi}[\cos(\frac{\pi n}{\tau}a) - \cos(\frac{\pi n}{\tau}b) \\ &+ \cos(n\pi + \frac{\pi n}{\tau}b) - \cos(n\pi - \frac{\pi n}{\tau}a)] \end{aligned} \tag{4.12}$$

Substituting Equation 4.12 into Equation 4.11 we get:

$$B(\theta) = \frac{4B_m}{\pi} \sum_{n=1,3,5...}^{\infty} [\cos(\frac{\pi n}{\tau}a) - \cos(\frac{\pi n}{\tau}b)] \frac{\sin(\frac{\pi n}{\tau}\theta)}{n} \tag{4.13}$$

From Equation 4.13 it becomes evident that if a term is zero for a value of n, the n'th harmonic will be removed. The distribution of the PM flux density in the centre outer air-gap was measured. The magnitude of the r-component was recorded for a distance of two pole-pitches. The harmonics are shown in Figure 4.32. It is not necessary to remove the third harmonic as its influence is mitigated by the winding arrangement[4]. The next two largest harmonics are the fifth and seventh, thus n was appropriately chosen resulting in the following equations:

$$B(\theta)_5 = \frac{4B_m}{\pi}[\cos(\frac{5\pi}{\tau}a) - \cos(\frac{5\pi}{\tau}b)] \frac{\sin(\frac{5\pi}{\tau}\theta)}{5} = 0 \tag{4.14}$$

$$B(\theta)_7 = \frac{4B_m}{\pi}[\cos(\frac{7\pi}{\tau}a) - \cos(\frac{7\pi}{\tau}b)]\frac{\sin(\frac{7\pi}{\tau}\theta)}{7} = 0 \tag{4.15}$$

Solving equations 4.14 and 4.15 would give the necessary values for a and b to remove the fifth and seventh harmonics. These values are $a = \frac{6\tau}{70}$ and $b = \frac{34\tau}{70}$.However, approximating $a = \frac{\tau}{10}$ and $b = \frac{\tau}{2}$ would produce a magnet with a width of 80 % of the pole pitch, thus confirming the results obtained by Joseph [15]. Both magnet configurations were tested. The flux density for each configuration was measured and the harmonic content is shown in Figure 4.32. Reducing the magnet size reduces the fundamental of the flux density, which will reduce the thrust force of the machine.

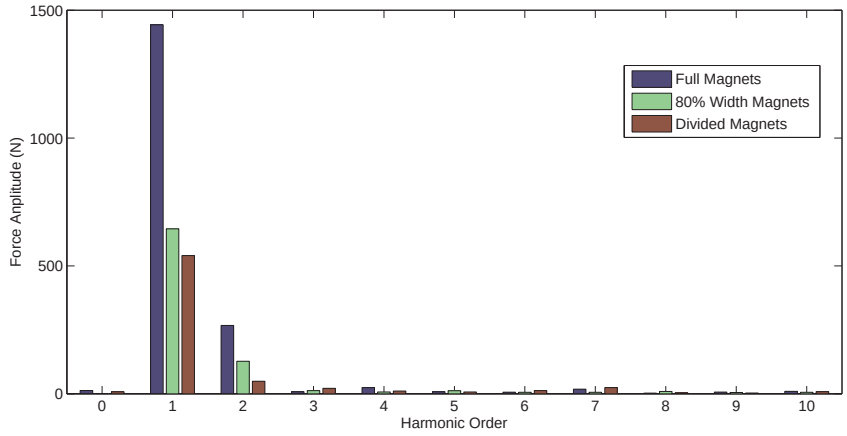

Figure 4.31: Slot Cogging Harmonic Content of the Original Magnets, Magnets with 80% Width and Divided Magnets.

The actual slot cogging forces were approximated by measuring the force acting on the translator and subtracting the stator ends forces. Only the PMs produced flux for this test. Consequently the peak flux intensity was below saturation values. The stator was moved across two slot pitches in increments of $\frac{\tau_s}{256}$, while the slot cogging force was calculated for each position. The simulation was done for magnets with a width of 80% of the pole pitch, divided magnets and full width magnets as a reference. The harmonic content of each result is shown in Figure 4.31. Reducing the magnets' width to 80% of a pole pitch makes a substantial difference, thereby reducing the fundamental and second harmonics by more than half. However, further dividing the magnets into two pieces did not make a significant impact on the fundamental, but reduced the second harmonic by a further half.

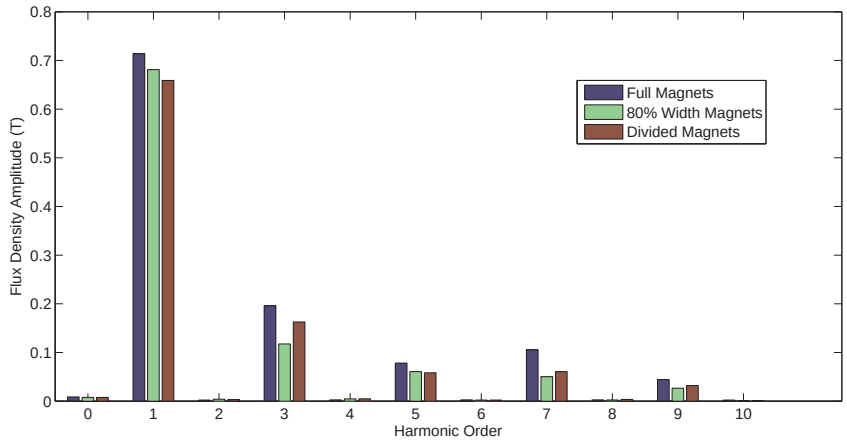

Figure 4.32: Flux Density Harmonic Content of the Original Magnets, Magnets with 80% Width and Divided Magnets.

4.2.3 Magnet Offset

The total slot cogging force is a combination of the slot cogging forces of the inner and outer stators. These forces are in phase due to the design of the machine, thus compounding for the total effect. Each set of PMs on either side of the translator back-iron is largely affected by the stator on the same side. Shifting either set of PMs should thus shift its cogging force by a similar amount. This logic is based on the technique used to cancel the end effects force. The largest component of the slot cogging force is the fundamental, which has a period of $2\tau_s$ ($\tau_s = 1$ cm).

The PMs opposite the outer stator was shifted by 1 cm in the z-direction (shown in Figure 4.34). Simulations were done for magnets with 80% width and divided magnets. The results are shown in Figure 4.33.

4.3 Effect of Reduction Methods on the Machine Performance

The overall performance of the DSTLPMG is measured by its force density and material utilisation. The original design boasts a higher force density in comparison to a flat layout. Unfortunately, the new combination of a double-sided and tubular layout results in an increased stator end-face area which increases the end effects cogging force. It also doubles the amount of stator slots, which increases the slot cogging force. This chapter has shown that the cogging forces can be reduced. These

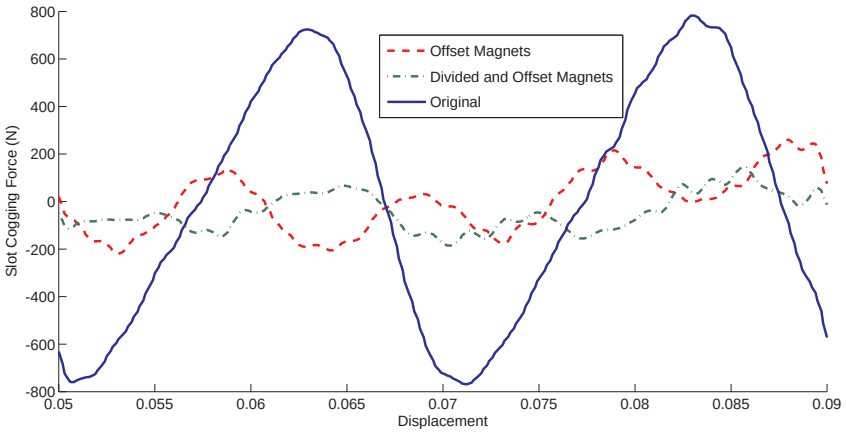

Figure 4.33: Slot Cogging Force of the Original Magnets, Shifted Magnets, and Shifted and Divided Magnets.

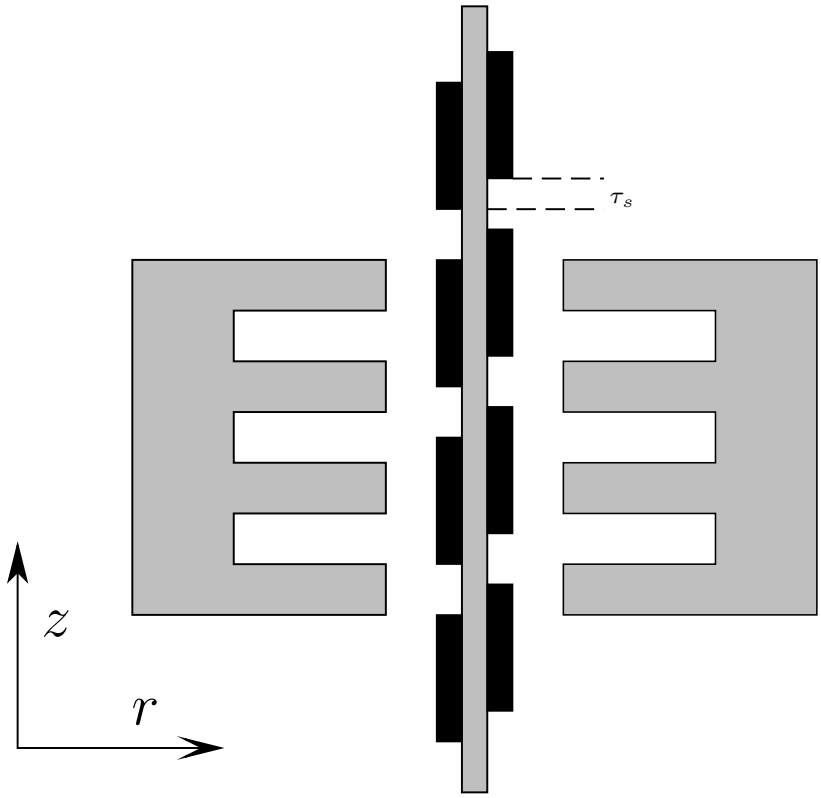

Figure 4.34: Arrangement of shifted PMs.

reduction methods, however, either require additional materials or a reduction of the PM size. Figure 4.35 shows the translator force after the stator length has been optimised,the stator ends have been shaped like a bézier curve, and the magnets were divided and shifted by one slot pitch. Figure 4.36 shows the harmonic content for the translator force of the original and modified machine.

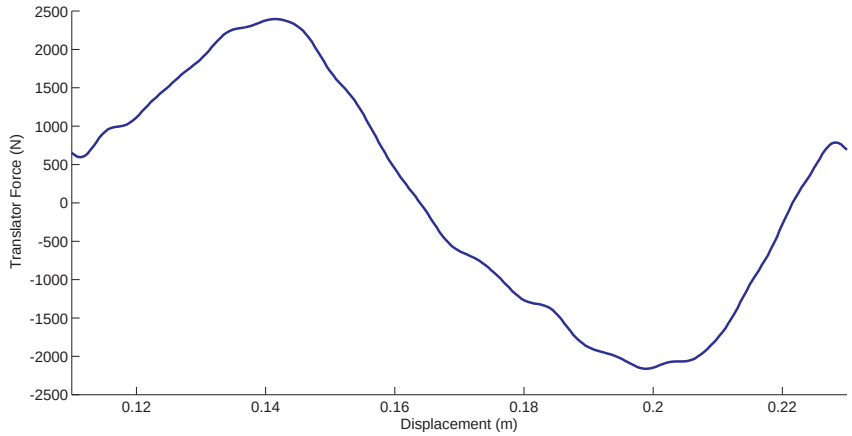

Figure 4.35: Translator Force (After Cogging Force Reduction Methods Have Been Applied).

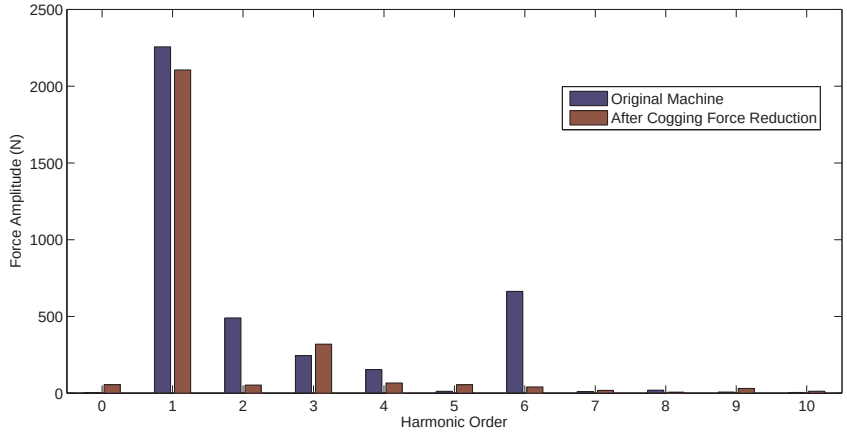

Figure 4.36: Harmonic Content of the Translator Force (Original and Modified Machine).

4.3.1 End Effect Reduction Changes

These methods for reducing the end effect cogging forces require that the stator length be increased, as well as the stator end face shape be changed. This increases the machine volume and reduces the force density. A compromise, however, needs to be made between the machine volume and peak cogging force reduction involved with each method. Table 4.1 summarises the results.

Table 4.1: Summary of End Effect Reduction Methods Results.

Reduction Method	Volume	Peak Cogging Force
Original Machine	22.27×10^{-3} m^3	630 N
Increased Stator Length	24.04×10^{-3} m^3	233 N
Triangular Stator End Shape	27.7×10^{-3} m^3	61 N
Bézier Curve Stator End Shape	27.82×10^{-3} m^3	7 N
Stepped Stator End Shape	23.67×10^{-3} m^3	22 N

4.3.2 Slot Cogging Reduction Changes

The changes made to reduce slot cogging forces were: Firstly, dividing the magnets and ,secondly,offsetting the outer magnets relative to the inner magnets. The first change reduces the machine volume marginally, but also reduces the fundamental component of the air-gap flux density. This in turn reduces the thrust force. There again is a compromise to be made between reduction of the slot cogging force (sixth harmonic) and not reducing the thrust force (fundamental). A summary of the results is shown in Table 4.2.

Table 4.2: Summary of Slot Cogging Reduction Methods Results.

Reduction Method	Thrust Force	Slot Cogging Force
Original Machine	2260 N	663 N
Shifted Magnets	2160 N	11 N
Divided Magnets	2230 N	445 N
Divided and Shifted Magnets	2150 N	25 N

4.4 Conclusion

This chapter was centred around the description and reduction of cogging forces. Linear machines suffer from cogging forces generated by two different mechanisms. End effect cogging forces are composed of two forces acting on the stator ends. These forces are mirror images of each other and are generated by the interaction of the

PMs and the stator ends. The phase shift between the two forces is dependent on the stator length. Slot cogging forces arise from the interaction of the PMs and the stator slots.

The peak end effect cogging force of the DSTLPMG was 630 N, the fundamental was removed by changing the stator length in order for the fundamentals of two forces acting on the stator ends to be eliminated. The second harmonic was removed by altering the stator end shapes. Three different shapes were presented: triangular, quadratic bézier curve and a rectangular step shape. The size of of the shapes were optimized to minimise the second harmonic component. The bézier curve shape resulted in the largest cogging force reduction, reducing the peak cogging force to 7 N. This, however, increased the machine volume to 27.82×10^{-3} m^3. The rectangular step shape produced the best overall result, the peak cogging force was reduced to 22 N and the machine volume increased to 23.67×10^{-3} m^3.

Slot cogging forces were reduced by two methods, dividing the PMs into sections to remove certain harmonics from the air-gap flux distribution and offsetting the outer PMs relative to the inner PMs in order for the inner and outer slot cogging forces to be eliminated. Dividing the PMs reduced the slot cogging force from 663 N to 445 N, offsetting the PMs reduced the slot cogging force to 11 N.

Chapter 5

Conclusions

Excessive cogging forces have a negative impact on the performance of generators. The purpose of this research was to improve the design of a DSTLPMG in order for it to perform adequately during dynamic tests and subsequent normal operation. A DSTLPMG designed by D. Joseph was simulated and static forces were measured using ANSYS and COMSOL. The analysis of these results led to the identification of significant forces ripples. These ripples are due to the interaction of the PMs and stator steel sections. Two mechanism for producing the force ripples were identified, end-effects and slot cogging. The end effect cogging force was reduced using two different techniques. Firstly, by resizing the stator, the fundamental harmonic was eliminated, and, secondly, by shaping the stator ends, the second harmonic was reduced. The slot cogging forces were reduced by dividing the PMs into two sections and offsetting the outer PMs relative to the inner PMs.

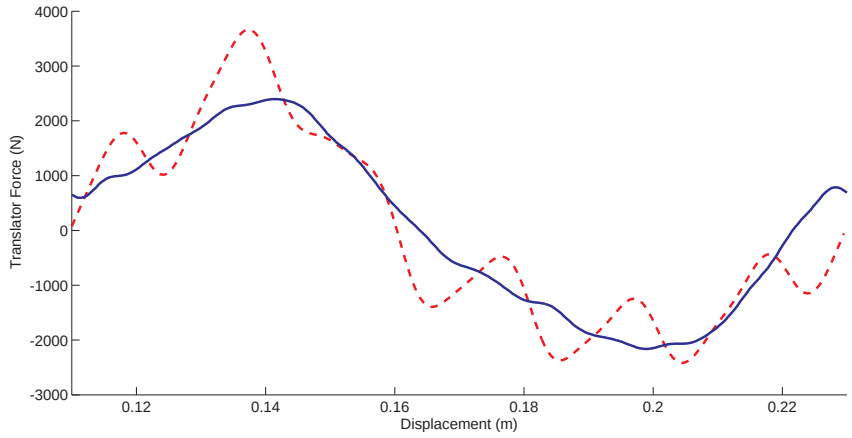

Figure 5.1: Translator Force of the Original Machine vs. the Optimised Machine.

Figure 5.1 shows the difference between the translator force of the original machine after optimisations were applied. These optimisations are:

1 The stator end shapes were changed to a quadratic bézier curve.

2 The stator length was increased, the magnets were divided into two pieces and offset by one slot pitch.

Tables 5.1 and 5.2 show the effect on the machine volume and thrust force by different cogging force reduction techniques. This, however, a compromise between performance and cogging force reduction.

Table 5.1: Summary of End Effect Reduction Methods Results.

Reduction Method	Volume	Peak Cogging Force
Original Machine	22.27×10^{-3} m^3	630 N
Increased Stator Length	24.04×10^{-3} m^3	233 N
Triangular Stator End Shape	27.7×10^{-3} m^3	61 N
Bézier Curve Stator End Shape	27.82×10^{-3} m^3	7 N
Stepped Stator End Shape	23.67×10^{-3} m^3	22 N

Table 5.2: Summary of Slot Cogging Reduction Methods Results.

Reduction Method	Thrust Force	Slot Cogging Force
Original Machine	2260 N	663 N
Shifted Magnets	2160 N	11 N
Divided Magnets	2230 N	445 N
Divided and Shifted Magnets	2150 N	25 N

5.1 Proposals for Future Research

Even though this research has improved the design of the machine by reducing cogging forces, further efforts to optimize the design can be undertaken. The

above results were not validated by experimental work. Pure analytical methods of designing machines are invaluable as a first step because it saves resources otherwise wasted on iterations of designs having to be built and tested. However, when a certain level of confidence is reached in with an analytical design, it must be validated with a physical model to account for non-ideal, real world conditions. The author believes that the next step is to build a scaled down model and perform static force testing to validate the results.

In-depth mechanical analysis and optimisation is required in conjunction with an investigation into alternative magnetic materials. By using Soft Magnetic Composites (SMCs) semi-closed stator slots can easily be fashioned. SMCs can be moulded into arbitrary shapes making it easier to manufacture round stator ends. Due to the composition of SMCs, eddy currents are negligible, which removes the need for lamination stacks.

References

[1] S. Barstow, G. Mrk, L. Lnseth, and J. Mathisen, "Worldwaves wave energy resource assessments from the deep ocean to the coast," in *8th European Wave and Tidal Energy Conference*, 2009, pp. 149–159.

[2] R. Boud, "Status and research and development priorities — 2003 wave and marine current energy," INTERNATIONAL ENERGY AGENCY, Tech. Rep., 2003.

[3] D. J. Whitford, "Teaching ocean wave forecasting using computer-generated visualization and animationpart 1: sea forecasting," *Computers & geosciences*, vol. 28, p. 537546, 2002.

[4] D. M. Joseph, "A double-sided tubular linear synchronous generator for wave-energy conversion," Ph.D. dissertation, University of the Witwatersrand, Johannesburg, 2009.

[5] J. Falnes, "A review of wave-energy extraction," *Marine Structures*, vol. 20, pp. 185–201, 2007.

[6] A. F. D. O. Falcão, "Wave energy utilization: A review of the technologies," *Renewable and Sustainable Energy Reviews*, vol. 14, pp. 899–918, 2010.

[7] J. Joubert, "An investigation of the wave energy resource on the south african coast , focusing on the spatial distribution of the south west coast," Master's thesis, Civil Engineering, University of Stellenbosch, 2008.

[8] A. Muetze and J. Vining, "Ocean wave energy conversion-a survey," in *Industry Applications Conference, 2006. 41st IAS Annual Meeting. Conference Record of the 2006 IEEE*, 2006.

[9] H. Polinder and M. Scuotto, "Wave energy converters and their impact on power systems," in *Future Power Systems, 2005 International Conference on*, 2005.

[10] J. G. Vining and A. Muetze, "Economic factors and incentives for ocean wave energy conversion," *IEEE Transactions on Industry Applications*, vol. 45, pp. 547–554, 2009.

[11] J. F. Gieras and Z. J. Piech, *Linear Synchronous Motors - Transportation and Automation Systems*. CRC Press LLC, 2000 N.W. Corporate Blvd., Boca Raton, Florida 33431, 2000.

[12] C. A. Oprea, C. S. Martis, F. N. Jurca, D. Fodorean, L. Szabo, and L. Szab, "Permanent magnet linear generator for renewable energy applications: Tubular vs. four-sided structures," in *2011 International Conference on Clean Electrical Power (ICCEP)*, 2011.

[13] H. Polinder, M. Damen, and F. Gardner, "Linear pm generator system for wave energy conversion in the aws," *IEEE Transactions on Energy Conversion*, vol. 19, pp. 583–589, 2004.

[14] P. Sen, *Principles of Electric Machines and Power Electronics*. John Wiley & Sons, 1997.

[15] D. Joseph and W. Cronje, "Design of a double-sided tubular permanent-magnet linear synchronous generator for wave-energy conversion," *COMPEL: The International Journal for Computation and Mathematics in Electrical and Electronic Engineering*, vol. 27, no. 1, pp. 154–169, 2008.

[16] Y. wu Zhu, S.-G. Lee, K.-S. Chung, and Y.-H. Cho, "Investigation of auxiliary poles design criteria on reduction of end effect of detent force for pmlsm," *Magnetics, IEEE Transactions on*, vol. 45, pp. 2863–2866, 2009.

[17] D. Howe and G. Jewell, "Fringing in tubular permanent-magnet machines: part ii. cogging force and its minimization," *Magnetics, IEEE Transactions on*, vol. 39, no. 6, pp. 3517–3522, Nov. 2003.

[18] N. Kimoulakis, A. Kladas, and J. Tegopoulos, "Cogging force minimization in a coupled permanent magnet linear generator for sea wave energy extraction applications," *Magnetics, IEEE Transactions on*, vol. 45, no. 3, pp. 1246–1249, 2009.

[19] I. Ivanova, O. Agren, H. Bernhoff, and M. Leijon, "Simulation of cogging in a 100 kw permanent magnet octagonal linear generator for ocean wave conversion," in *Underwater Technology, 2004. UT '04. 2004 International Symposium on*, 2004, pp. 345 –348.

[20] O. Danielsson and M. Leijon, "Flux distribution in linear permanent-magnet synchronous machines including longitudinal end effects," *Magnetics, IEEE Transactions on*, vol. 43, no. 7, pp. 3197–3201, 2007.

[21] Z. Zhu, Z. Xia, D. Howe, and P. Mellor, "Reduction of cogging force in slotless linear permanent magnet motors," *Electric Power Applications, IEE Proceedings* -, vol. 144, no. 4, pp. 277 –282, Jul. 1997.

[22] M. Inoue and K. Sato, "An approach to a suitable stator length for minimizing the detent force of permanent magnet linear synchronous motors," *Magnetics, IEEE Transactions on*, vol. 36, no. 4, pp. 1890–1893, Jul. 2000.

[23] J. Wang, M. Inoue, Y. Amara, and D. Howe, "Cogging-force-reduction techniques for linear permanent-magnet machines," *Electric Power Applications, IEE Proceedings* -, vol. 152, no. 3, pp. 731–738, May 2005.

[24] T. Theoharis, G. Papaioannou, N. Platis, and N. M. Patrikalakis, *Graphics and Visualization: Principles & Algorithms*. A K Peters/CRC Press, 2007.

[25] Y. Yang, X. Wang, C. Zhu, and C. Huang, "Study of magnet asymmetry for reduction of cogging torque in permanent magnet motors," in *Proc. 4th IEEE Conf. Industrial Electronics and Applications ICIEA 2009*, 2009, pp. 2325–2328.

[26] T. M. Jahns and W. L. Soong, "Pulsating torque minimization techniques for permanent magnet ac motor drives-a review," *IEEE Transactions on Industrial Electronics*, vol. 43, no. 2, pp. 321–330, 1996.

[27] M.-Y. Kim, Y.-C. Kim, and G.-T. Kim, "Design of slotless-type pmlsm for high power density using divided pm," *IEEE Transactions on Magnetics*, vol. 40, pp. 746–749, 2004.

Appendix A

Mathematical Expansions

A.1 Derivation of Total End-Effects Force

$$
\begin{aligned}
F &= F_{top} + F_{bottom} \\
&= \sum_{n=1}^{\infty} F_{sn} \sin(\frac{2\pi n}{\tau} z) + \sum_{n=1}^{\infty} F_{cn} \cos(\frac{2\pi n}{\tau} z) \\
&\quad + \sum_{n=1}^{\infty} F_{sn} \sin(\frac{2\pi n}{\tau}(z+\delta)) - \sum_{n=1}^{\infty} F_{cn} \cos(\frac{2\pi n}{\tau}(z+\delta))
\end{aligned} \tag{A.1}
$$

Let $A = \frac{2\pi n}{\tau} z$ and $B = \frac{2\pi n}{\tau} \delta$

$$
\begin{aligned}
&= \sum_{n=1}^{\infty} [F_{sn}(\sin(A) + \sin(A+B)) + F_{cn}(\cos(A) - \cos(A+B))] \\
&= \sum_{n=1}^{\infty} [F_{sn}(\sin((A + \frac{B}{2}) - \frac{B}{2}) + \sin((A + \frac{B}{2}) + \frac{B}{2})) \\
&\quad + F_{cn} \cos((A + \frac{B}{2}) - \frac{B}{2}) - \cos((A + \frac{B}{2}) + \frac{B}{2}))]
\end{aligned}
$$

Using: $\sin(u)\cos(v) = \frac{\sin(u-v)+\sin(u+v)}{2}$

and $\sin(u)\sin(v) = \frac{\cos(u-v)-\cos(u+v)}{2}$

$$= \sum_{n=1}^{\infty} [2F_{sn} \sin(A + \frac{B}{2}) \cos(\frac{B}{2}) + 2F_{cn} \sin(A + \frac{B}{2}) \sin(\frac{B}{2})]$$

Substituting back in for A and B

$$= \sum_{n=1}^{\infty} 2[F_{sn} \cos(\frac{n\pi}{\tau}\delta) + F_{cn} \sin(\frac{n\pi}{\tau}\delta)] \sin(\frac{2\pi n}{\tau}(z + \delta/2))$$

Appendix B

Source Code Listing

Listing B.1: Machine Simulation Script in Ansys.

```
/TITLE, Wave-Gen basic simulation
/NOPR


! Number of iterations for in force do loop.
nite = 1
*dim, offset, table, nite
*dim, frs, table, nite
d = 0

*DO, ite, 1, nite
PARSAV, ALL
/CLEAR, NOSTART
PARRES

/com, d = %d%

/PREP7

ET, 1, PLANE53            ! Define PANE53 as an element type.
KEYOPT, 1, 3, 1           ! Use axisymmetric analysis option.
ET, 2, 169
ET, 3, 172, 7, 2,,2
KEYOPT, 3, 12, 5


MP, MURX, 1, 1            ! Permeability of air.

! Create a B-H curve for the back-iron steel.
TB, BH, 2,, 60
TBPT,,0, 0
,,9.510307, 0.004445
,,11.21247, 0.005819
,,13.219414, 0.007193
,,15.585253, 0.008568
,,18.371262, 0.012898
,,21.656221, 0.017228
,,25.5213, 0.02747
,,30.061992, 0.046579
,,35.364241, 0.092289
,,41.430434, 0.22076
,,48.386303, 0.4113
,,56.51037, 0.60185
,,66.066036, 0.7717
```

```
,,77.340576, 0.91495
,,90.591026, 1.0464
,,106.212089, 1.1601
,,124.594492, 1.2619
,,146.311191, 1.3431
,,172.06247, 1.3947
,,202.524737, 1.4286
,,238.525598, 1.4507
,,281.012026, 1.4668
,,331.058315, 1.483
,,390.144609, 1.4932
,,459.695344, 1.5064
,,541.731789, 1.5167
,,638.410494, 1.5269
,,752.333643, 1.5372
,,886.572927, 1.5474
,,1044.772997, 1.5576
,,1231.22308, 1.5679
,,1450.53867, 1.584
,,1709.165545, 1.5972
,,2013.867792, 1.6104
,,2372.523585, 1.6266
,,2795.159688, 1.6427
,,3292.996527, 1.6589
,,3878.92566, 1.678
,,4569.101317, 1.6971
,,5382.065058, 1.7162
,,6339.700693, 1.7353
,,7465.563162, 1.7604
,,8791.7222, 1.7854
,,10352.23698, 1.8104
,,12188.88568, 1.8384
,,14347.82325, 1.8723
,,16887.93705, 1.9061
,,19872.0933, 1.9459
,,23380.66528, 1.9887
,,27504.37133, 2.0344
,,32364.96503, 2.0742
,,38095.3408, 2.1081
,,44847.49168, 2.139
,,52819.56563, 2.1611
,,62227.21768, 2.1772
,,73321.11695, 2.1904
!MP, MURX, 2, 2500

! Permeability of laminated steel.
TB, BH, 3,, 60
TBPT,,0, 0
,,9.510307, 0.004445
,,11.21247, 0.005819
,,13.219414, 0.007193
,,15.585253, 0.008568
,,18.371262, 0.012898
,,21.656221, 0.017228
,,25.5213, 0.02747
,,30.061992, 0.046579
,,35.364241, 0.092289
,,41.430434, 0.22076
,,48.386303, 0.4113
,,56.51037, 0.60185
,,66.066036, 0.7717
,,77.340576, 0.91495
,,90.591026, 1.0464
,,106.212089, 1.1601
,,124.594492, 1.2619
```

```
,,146.311191, 1.3431
,,172.06247, 1.3947
,,202.524737, 1.4286
,,238.525598, 1.4507
,,281.012026, 1.4668
,,331.058315, 1.483
,,390.144609, 1.4932
,,459.695344, 1.5064
,,541.731789, 1.5167
,,638.410494, 1.5269
,,752.333643, 1.5372
,,886.572927, 1.5474
,,1044.772997, 1.5576
,,1231.22308, 1.5679
,,1450.53867, 1.584
,,1709.165545, 1.5972
,,2013.867792, 1.6104
,,2372.523585, 1.6266
,,2795.159688, 1.6427
,,3292.996527, 1.6589
,,3878.92566, 1.678
,,4569.101317, 1.6971
,,5382.065058, 1.7162
,,6339.700693, 1.7353
,,7465.563162, 1.7604
,,8791.7222, 1.7854
,,10352.23698, 1.8104
,,12188.88568, 1.8384
,,14347.82325, 1.8723
,,16887.93705, 1.9061
,,19872.0933, 1.9459
,,23380.66528, 1.9887
,,27504.37133, 2.0344
,,32364.96503, 2.0742
,,38095.3408, 2.1081
,,44847.49168, 2.139
,,52819.56563, 2.1611
,,62227.21768, 2.1772
,,73321.11695, 2.1904

!MP, MURY, 3, 500          ! Permeability of laminated steel in
    Y-direction.
!MP, MURX, 3, 0            ! Use the B-H curve.

! Set permeabilities for each phase coil.
MP, MURX, 4, 1             ! Inner stator positive phase A.
MP, MURX, 5, 1             ! Inner stator negative phase A.
MP, MURX, 6, 1             ! Inner stator positive phase B.
MP, MURX, 7, 1             ! Inner stator negative phase B.
MP, MURX, 8, 1             ! Inner stator positive phase C.
MP, MURX, 9, 1             ! Inner stator negative phase C.

MP, MURX, 10, 1            ! Outer stator positive phase A.
MP, MURX, 11, 1            ! Outer stator negative phase A.
MP, MURX, 12, 1            ! Outer stator positive phase B.
MP, MURX, 13, 1            ! Outer stator negative phase B.
MP, MURX, 14, 1            ! Outer stator positive phase C.
MP, MURX, 15, 1            ! Outer stator negative phase C.


MP, MURX, 16, 1.034        ! Permeability of permanent magnets (left
    facing north pole).
MP, MGXX, 16, -960000      ! Magnetic coersive force of above magnet.
MP, MURX, 17, 1.034        ! Permeability of permanent magnets (right
    facing north pole).
```

```
MP, MGXX, 17, 960000      ! Magnetic coersive force of above magnet.

! Permeability if translator back iron steel.
TB, BH, 18,, 60
TBPT,,0, 0
,,9.510307, 0.004445
,,11.21247, 0.005819
,,13.219414, 0.007193
,,15.585253, 0.008568
,,18.371262, 0.012898
,,21.656221, 0.017228
,,25.5213, 0.02747
,,30.061992, 0.046579
,,35.364241, 0.092289
,,41.430434, 0.22076
,,48.386303, 0.4113
,,56.51037, 0.60185
,,66.066036, 0.7717
,,77.340576, 0.91495
,,90.591026, 1.0464
,,106.212089, 1.1601
,,124.594492, 1.2619
,,146.311191, 1.3431
,,172.06247, 1.3947
,,202.524737, 1.4286
,,238.525598, 1.4507
,,281.012026, 1.4668
,,331.058315, 1.483
,,390.144609, 1.4932
,,459.695344, 1.5064
,,541.731789, 1.5167
,,638.410494, 1.5269
,,752.333643, 1.5372
,,886.572927, 1.5474
,,1044.772997, 1.5576
,,1231.22308, 1.5679
,,1450.53867, 1.584
,,1709.165545, 1.5972
,,2013.867792, 1.6104
,,2372.523585, 1.6266
,,2795.159688, 1.6427
,,3292.996527, 1.6589
,,3878.92566, 1.678
,,4569.101317, 1.6971
,,5382.065058, 1.7162
,,6339.700693, 1.7353
,,7465.563162, 1.7604
,,8791.7222, 1.7854
,,10352.23698, 1.8104
,,12188.88568, 1.8384
,,14347.82325, 1.8723
,,16887.93705, 1.9061
,,19872.0933, 1.9459
,,23380.66528, 1.9887
,,27504.37133, 2.0344
,,32364.96503, 2.0742
,,38095.3408, 2.1081
,,44847.49168, 2.139
,,52819.56563, 2.1611
,,62227.21768, 2.1772
,,73321.11695, 2.1904
!MP, MURX, 18, 2500


! Define stator currents.
```

```
ISA     = 4.2                    ! Inner stator phase A current.
ISB     = 4.2/2                  ! Inner stator phase B current.
ISC     = 4.2/2                  ! Inner stator phase C current.

OSA     = 40.2                   ! Outer stator phase A current.
OSB     = 40.2/2                 ! Outer stator phase B current.
OSC     = 40.2/2                 ! Outer stator phase C current.

NIS     = 80                   ! Number of turns(inner stator).
NOS     = 14                   ! Number of turns(outer stator).

! Set geometric parameters.
TBIIR   = 0.073                ! Translator Back Iron Inner Radius.
TBIW    = 0.005                ! Translator Back Iron Width.
TBIH    = 1                    ! Translator Back Iron Height.
TBIBC   = 0                    ! Translator Back Iron bottom coordinate.

ISBIIR = 0.003                 ! Inner Stator Back Iron Inner Radius.
ISBIW   = 0.0335               ! Inner Stator Back Iron Thickness.
ISBIH   = 0.36                 ! Inner Stator Back Iron Height.

OSBIIR = 0.1238                ! Outer Stator Back Iron Inner Radius.
OSBIW   = 0.014                ! Outer Stator Back Iron Width.
OSBIH   = 0.36                 ! Outer Stator Back Iron Height.

ISIR    = 0.0365               ! Inner Stator Inner Radius.
OSIR    = 0.08748              ! Outer Stator Inner Radius.

ISCW    = 0.027                ! Inner Stator Coil Width.
ISCH    = 0.01                 ! Inner Stator Coil Height.

OSCW    = 0.03632              ! Outer Stator Coil Width.
OSCH    = 0.01                 ! Outer Stator Coil Height.

ISLSW   = 0.027                ! Inner Stator Lamination Stack Width.
ISLSH   = 0.01                 ! Inner Stator Lamination Stack Height.

OSLSW   = 0.03632              ! Outer Stator Lamination Stack Width.
OSLSH   = 0.01                 ! Outer Stator Lamination Stack Height.

PMW     = 0.005                ! Permanent Magnet Width.
PMH     = 0.048                ! Permanent Magnet Height.
PMBP    = TBIBC + 0.032        ! Permanent Magnet Bottom Position, ie.
    gap between
                               ! lowest PM and bottom of translator
                                  back iron.
PMG     = 0.012                ! Permanent Magnet Gap, ie gap between
    PM's

IPMIR   = 0.068                ! Inner Permanent Magnet Inner Radius.
OPMIR   = 0.078                ! Outer Permanent Magnet Inner Radius.

ISCS    = 36                   ! Number of Inner Stator Coils
ISLS    = 37                   ! Number of Inner Stator Lamination
    Stacks.
OSCS    = 36                   ! Number of Outer Stator Coils.
OSLS    = 37                   ! Number of Outer Stator Lamination
    Stacks.

/com, ite = %ite%
offset(ite) = d
SOS      = d                 ! Stator offset.
!SOS      = 0                  ! Stator offset.
d        = d + 0.1/(nite)
```

```
! Calculate curent densities(AT/m^2).
JIA = (ISA*NIS/(ISCW*ISCH))
JIB = (ISB*NIS/(ISCW*ISCH))
JIC = (ISC*NIS/(ISCW*ISCH))

JOA = (OSA*NOS/(OSCW*OSCH))
JOB = (OSB*NOS/(OSCW*OSCH))
JOC = (OSC*NOS/(OSCW*OSCH))

/PNUM, AREA, 1                ! Start the area numbering from 1.

! Do not change!
SOS = SOS+0.01

! Create the translator back iron.
RECTNG, TBIIR, TBIIR+TBIW, TBIBC+0.01, TBIBC+TBIH+0.01

! Create the inner stator back iron.
RECTNG, ISBIIR, ISBIIR+ISBIW, SOS, SOS+ISBIH

! Create the outer stator back iron.
RECTNG, OSBIIR, OSBIIR+OSBIW, SOS, SOS+OSBIH

! Create the inner stator lamination stacks.
*DO, I, 0, 35, 2
RECTNG, ISIR, ISIR+ISLSW, SOS+I*ISLSH, SOS+(I*ISLSH)+ISLSH
*ENDDO

! Create the outer stator lamination stacks.
*DO, I, 0, 35, 2
RECTNG, OSIR, OSIR+OSLSW, SOS+I*OSLSH, SOS+(I*OSLSH)+OSLSH
*ENDDO

! Create the inner stator coils.
*DO, I, 1, 36, 2
RECTNG, ISIR, ISIR+ISCW, SOS+I*ISCH, SOS+(I*ISCH)+ISCH
*ENDDO

! Create the outer stator coils.
*DO, I, 1, 36, 2
RECTNG, OSIR, OSIR+OSCW, SOS+I*OSCH, SOS+(I*OSCH)+OSCH
*ENDDO

! Create the inner magnets with left facing north poles.
*DO, I, 0, 9, 2
RECTNG, IPMIR, IPMIR+PMW, PMBP+I*(PMH+PMG), PMBP+I*(PMH+PMG)+PMH
*ENDDO

! Create the outer magnets with left facing north poles.
*DO, I, 0, 9, 2
RECTNG, OPMIR, OPMIR+PMW, PMBP+I*(PMH+PMG), PMBP+I*(PMH+PMG)+PMH
*ENDDO

! Create the inner magnets with right facing north poles.
*DO, I, 1, 9, 2
RECTNG, IPMIR, IPMIR+PMW, PMBP+I*(PMH+PMG), PMBP+I*(PMH+PMG)+PMH
*ENDDO

! Create the outer magnets with right facing north poles.
*DO, I, 1, 9, 2
RECTNG, OPMIR, OPMIR+PMW, PMBP+I*(PMH+PMG), PMBP+I*(PMH+PMG)+PMH
*ENDDO

! Create the air enclosure.
RECTNG, 0, OSBIIR+OSBIW+0.01, 0, TBIH+0.015
```

```
! AND all overlapping areas.
AOVLAP, ALL

! Compress out all unused numbers and replot.
NUMCMP, AREA

K,, ISIR+ISCW, TBIBC
K,, ISIR+ISCW, TBIH+0.015

K,, OSIR, TBIBC
K,, OSIR, TBIH+0.015

L, 13, 86
L, 157, 158

ASBL, 96, 2,,,DELETE
ASBL, 98, 4,,,DELETE

NUMCMP, AREA

ASEL, ALL
APLOT

! Select areas and assign material attributes.

! Stator lamination sections.
ASEL, S, AREA,, 55
ASEL, A, AREA,, 1, 34
ASEL, A, AREA,, 74
AATT, 3, 1, 1, 0

! Stator back irons.
ASEL, S, AREA,, 93, 94
AATT, 2, 1, 1, 0

! Translator back iron.
ASEL, S, AREA,, 95
AATT, 18, 1, 1, 0

! Air
ASEL, S, AREA,, 96, 98
AATT, 1, 1, 1, 0

! Magnets with left facing north poles.
ASEL, S, AREA,, 35, 44
AATT, 16, 1, 1, 0

! Magnets with right facing north poles.
ASEL, S, AREA,, 45, 54
AATT, 17, 1, 1, 0

! Inner stator coils A with positive current.
ASEL, S, AREA,, 61, 73, 6
AATT, 4, 1, 1, 0

! Inner stator coils B with positive current.
ASEL, S, AREA,, 60, 72, 6
AATT, 6, 1, 1, 0

! Inner stator coils C with positive current.
ASEL, S, AREA,, 59, 71, 6
AATT, 8, 1, 1, 0

! Inner stator coils A with negative current.
```

```
ASEL, S, AREA,, 58, 70, 6
AATT, 5, 1, 1, 0

! Inner stator coils B with negative current.
ASEL, S, AREA,, 57, 69, 6
AATT, 7, 1, 1, 0

! Inner stator coils C with negative current.
ASEL, S, AREA,, 56, 68, 6
AATT, 9, 1, 1, 0

! Outer stator coils A with positive current.
ASEL, S, AREA,, 80, 92, 6
AATT, 10, 1, 1, 0

! Outer stator coils B with positive current.
ASEL, S, AREA,, 79, 91, 6
AATT, 12, 1, 1, 0

! Outer stator coils C with positive current.
ASEL, S, AREA,, 78, 90, 6
AATT, 14, 1, 1, 0

! Outer stator coils A with negative current.
ASEL, S, AREA,, 77, 89, 6
AATT, 11, 1, 1, 0

! Outer stator coils B with negative current.
ASEL, S, AREA,, 76, 88, 6
AATT, 13, 1, 1, 0

! Outer stator coils C with negative current.
ASEL, S, AREA,, 75, 87, 6
AATT, 15, 1, 1, 0

ALLSEL, ALL
APLOT
/PNUM, MAT, 1
APLOT

!SMRTSIZE, 1                    ! Set smart size meshing level 1
    (finest)
! Select airgap area.
ASEL, S, AREA,, 98
ASEL, A, AREA,, 35, 54
ESIZE, 0.003
AMESH, ALL

! Select all the other areas.
ASEL, INVE
ESIZE, 0.009
AMESH, ALL

!ESLA, S
!NSLE, S
!NSEL, R, LOC, X, ISIR+ISCW
!TYPE, 2
!ESURF

!ESLA, S
!NSLE, S
!NSEL, R, LOC, X, OSIR
!TYPE, 2
!ESURF
```

```
!ASEL, INVE
!ESLA, S
!NSLE, S
!NSEL, R, LOC, X, ISIR+ISCW
!TYPE, 3
!ESURF

!ESLA, S
!NSLE, S
!NSEL, R, LOC, X, OSIR
!TYPE, 3
!ESURF


!ALLSEL, ALL
!AMESH, ALL                    ! Mesh all areas
ESEL, S, MAT,, 18              ! Select translator elements
!ESEL, A, MAT,, 16             ! Select permanent magnet elements
!ESEL, A, MAT,, 17             ! Select permanent magnet elements
CM, TRANS, ELEM                ! Define armature as a component
FMAGBC, 'TRANS'                ! Apply force boundary conditions to
    translator
ALLSEL, ALL
!ARSCALE, ALL,,,0.01,0.01,1,,,1  ! Scale model to MKS (meters)
FINISH

/SOLU

ESEL,S,MAT,,4                  ! Select coil elements phase A, positive
    current, inner stator
BFE,ALL,JS,,,,JIA  ! Apply current density (A/m**2)

ESEL,S,MAT,,6                  ! Select coil elements phase B, positive
    current, inner stator
BFE,ALL,JS,,,,JIB  ! Apply current density (A/m**2)

ESEL,S,MAT,,8                  ! Select coil elements phase C, positive
    current, inner stator
BFE,ALL,JS,,,,JIC  ! Apply current density (A/m**2)

ESEL,S,MAT,,5                  ! Select coil elements phase A, negative
    current, inner stator
BFE,ALL,JS,,,,-1*JIA   ! Apply current density (A/m**2)

ESEL,S,MAT,,7                  ! Select coil elements phase B, negative
    current, inner stator
BFE,ALL,JS,,,,-1*JIB  ! Apply current density (A/m**2)

ESEL,S,MAT,,9                  ! Select coil elements phase C,
    negative current, inner stator
BFE,ALL,JS,,,,-1*JIC  ! Apply current density (A/m**2)

ESEL,S,MAT,,10                 ! Select coil elements phase A, positive
    current, outer stator
BFE,ALL,JS,,,,JOA  ! Apply current density (A/m**2)

ESEL,S,MAT,,12                 ! Select coil elements phase B, positive
    current, outer stator
BFE,ALL,JS,,,,JOB  ! Apply current density (A/m**2)

ESEL,S,MAT,,14                 ! Select coil elements phase C, positive
    current, outer stator
BFE,ALL,JS,,,,JOC  ! Apply current density (A/m**2)
```

```
ESEL,S,MAT,,11                ! Select coil elements phase A, negative
    current, outer stator
BFE,ALL,JS,,,,-1*JOA  ! Apply current density (A/m**2)

ESEL,S,MAT,,13                ! Select coil elements phase B, negative
    current, outer stator
BFE,ALL,JS,,,,-1*JOB  ! Apply current density (A/m**2)

ESEL,S,MAT,,15                ! Select coil elements phase C, negative
    current, outer stator
BFE,ALL,JS,,,,-1*JOC  ! Apply current density (A/m**2)


NSEL, S, LOC, X, 0
NSEL, A, LOC, X, OSBIIR+OSBIW+0.01
NSEL, A, LOC, Y, 0
NSEL, A, LOC, Y, TBIH+0.015
D,ALL,AZ,0                    ! Set potentials to zero (flux-parallel)
ALLSEL,ALL
FINISH
/SOLU
NSUBST, 2, 5, 2, OFF
SOLCONTROL, ON
NEQIT, 30
MAGSOLV                       ! Solve magnetic field
SAVE

FINISH

/POST1
PLF2D                        ! Plot flux lines in the model

FMAGSUM                      ! Summarize magnetic forces
!SSUM
!*GET, FF, SSUM,, ITEM, FMX_Y
!frs(ite) = FF

!PLVECT,B,,,,VECT,ELEM,ON     ! Plot flux density as vectors
!/GRAPHICS,POWER              ! Turn PowerGraphics on
!AVRES,2                      ! Don't average results across materials
!PLNSOL,B,SUM                 ! Plot flux density magnitude
!/IMAGE, SAVE, 'C:\msc_img\ite%ite%', bmp
FINISH
*ENDDO
! Write the data to a file

*CFOPEN, 'reluctance_force_2_pole_pairs', txt
*VWRITE, offset(1), frs(1)
(F11.5, ',', F11.5)
*CFCLOS
*VPLOT, offset(1), frs(1)
```

Listing B.2: Calculation of δ.

```
function D = calculate_delta(y, num_harm)

% Remove the DC component.
y = remove_DC(y);

N=length(y(:, 2)');

% Compute the matrices of trigonometric functions
p=1:N/2+1;
n=1:N;
C=cos(2*pi*n'*(p-1)/N);
```

```
S=sin(2*pi*n'*(p-1)/N);

% Compute Fourier Coefficients
A=2/N*y(:, 2)'*C;
B=2/N*y(:, 2)'*S;
A(N/2+1)=A(N/2+1)/2;

% First get all the harmonics and then get rid of the
% sub-harmonics.

% DC offset.
FH(1) = abs(A(1)/2);     % Fake harmonics.

total_harmonics = length(A);
FH(2:total_harmonics) =
    sqrt(A(2:total_harmonics).*A(2:total_harmonics) +
    B(2:total_harmonics).*B(2:total_harmonics))./2;

% Find the fundamental, should be the first largest amplitude after
    DC.
if FH(1) == max(FH)
    temp_DC = FH(1);
    FH(1) = 0;
    fund_index = find(FH == max(FH));
    FH(1) = temp_DC;
else
    fund_index = find(FH == max(FH));
end

Fc = A(2:(fund_index-1):(fund_index-1)*(num_harm));
Fs = B(2:(fund_index-1):(fund_index-1)*(num_harm));

D(1:num_harm) =
    (0.06./(pi*(1:num_harm)))*atan(-1*(Fs(1:num_harm)/Fc(1:num_harm)));
```

Listing B.3: Filters Out Any High Order Harmonics.

```
function filter_signal(y, num, varargin)

N=length(y(:, 2)');

% Compute the matrices of trigonometric functions
p=1:N/2+1;
n=1:N;
C=cos(2*pi*n'*(p-1)/N);
S=sin(2*pi*n'*(p-1)/N);

% Compute Fourier Coefficients
A=2/N*y(:, 2)'*C;
B=2/N*y(:, 2)'*S;
A(N/2+1)=A(N/2+1)/2;

ynew=A(1)/2+C(:,2:num)*A(2:num)'+S(:,2:num)*B(2:num)';

% Plot reconstruction over data
hold on;
plot(y(:, 1), ynew);

% Plot the extra harmonics.
if size(varargin, 2) > 0
    for i =1:size(varargin, 2)
        plot(y(:, 1),
            A(1)/2+C(:,varargin{i})*A(varargin{i})'+S(:,varargin{i})*B(varargin{i})',
            'r');
    end
```

```
end

hold off;
```

Listing B.4: Plots the Harmonics of a Signal.

```
function H = plot_harmonics(y, num_harm, normalise)

N=length(y(:, 2)');

% Compute the matrices of trigonometric functions
p=1:N/2+1;
n=1:N;
C=cos(2*pi*n'*(p-1)/N);
S=sin(2*pi*n'*(p-1)/N);

% Compute Fourier Coefficients
A=2/N*y(:, 2)'*C;
B=2/N*y(:, 2)'*S;
A(N/2+1)=A(N/2+1)/2;

% First get all the harmonics and then get rid of the
% sub-harmonics.

% DC offset.
FH(1) = abs(A(1)/2);     % Fake harmonics.

total_harmonics = length(A);
FH(2:total_harmonics) =
    sqrt(A(2:total_harmonics).*A(2:total_harmonics) +
    B(2:total_harmonics).*B(2:total_harmonics))./2;

% Find the fundamental, should be the first largest amplitude after
    DC.
if FH(1) == max(FH)
    temp_DC = FH(1);
    FH(1) = 0;
    fund_index = find(FH == max(FH));
    FH(1) = temp_DC;
else
    fund_index = find(FH == max(FH));
end

% The rest of the harmonics should be multiples of the fundamental.
% Populate the real hamonics vector.
H(1:num_harm+1) = FH(1:(fund_index-1):(fund_index-1)*(num_harm+1));

if exist('normalise')
    if normalise == 1
        % Get the largest value;
        max_val = max(H);

        %Resize all the values.
        H = 100.*H./max_val;
    end
end

bar(0:num_harm, H, 0.3);
xlim(gca, [-1 (num_harm+1)]);
```

Listing B.5: Removes the DC Component of a Signal.

```
function y = remove_DC(x)
```

```
y(:, 1) = x(:, 1);
y(:, 2) = x(:, 2) - mean(x(:, 2));
```

Listing B.6: Converts a Matlab Figure to a pdf.

```
function save_plots()

% Get a list of all the figures in the 'figures' folder.
figures = dir('figures/*.fig');

for i = 1:numel(figures)
    [path, name, extension] = fileparts(['figures/',
        figures(i).name]);
    handle = open(['figures/', name, '.fig']);
    set(handle, 'paperunits', 'points');
    exportfig(handle, ['C:/Dropbox/thesis/graphics/', name, '.eps'],
        'width', 800, 'fontmode', 'fixed', 'fontsize', 12, 'color',
        'cmyk');
    close(handle);
    dos(['epstopdf C:/Dropbox/thesis/graphics/', name, '.eps']);
    dos('exit &');
    delete(['C:/Dropbox/thesis/graphics/', name, '.eps']);
end
```

Listing B.7: Plot the Calculated values of er.

```
function plot_er()

% Load all the variables into a structure.
er = load('data/shaped_end_top/er0_1.mat');

% Get the harmonic content of each signal
h005 = plot_harmonics(er.er005, 5);
h01 = plot_harmonics(er.er01, 5);
h015 = plot_harmonics(er.er015, 5);
h02 = plot_harmonics(er.er02, 5);
h025 = plot_harmonics(er.er025, 5);
h03 = plot_harmonics(er.er03, 5);
h035 = plot_harmonics(er.er035, 5);
h04 = plot_harmonics(er.er04, 5);
h045 = plot_harmonics(er.er045, 5);
h05 = plot_harmonics(er.er05, 5);
h055 = plot_harmonics(er.er055, 5);
h06 = plot_harmonics(er.er06, 5);
h065 = plot_harmonics(er.er065, 5);
h07 = plot_harmonics(er.er07, 5);
h075 = plot_harmonics(er.er075, 5);
h08 = plot_harmonics(er.er08, 5);
h085 = plot_harmonics(er.er085, 5);
h09 = plot_harmonics(er.er09, 5);
h095 = plot_harmonics(er.er095, 5);
h1 = plot_harmonics(er.er1, 5);

close all;

% x-axis vector
n = 0.05:0.05:1;

% Fundamental harmonic
h1 = [h005(2), h01(2), h015(2), h02(2), ...
      h025(2), h03(2), h035(2), h04(2), ...
      h045(2), h05(2), h055(2), h06(2), ...
      h065(2), h07(2), h075(2), h08(2), ...
      h085(2), h09(2), h095(2), h1(2)];
```

```
% 2'nd harmonic
h2 = [h005(3), h01(3), h015(3), h02(3), ...
     h025(3), h03(3), h035(3), h04(3), ...
     h045(3), h05(3), h055(3), h06(3), ...
     h065(3), h07(3), h075(3), h08(3), ...
     h085(3), h09(3), h095(3), h1(3)];

% 3'nd harmonic
h3 = [h005(4), h01(4), h015(4), h02(4), ...
      h025(4), h03(4), h035(4), h04(4), ...
      h045(4), h05(4), h055(4), h06(4), ...
      h065(4), h07(4), h075(4), h08(4), ...
      h085(4), h09(4), h095(4), h1(4)];

% Plot
hold on;
plot(n, h1);
plot(n, h2);
plot(n, h3);
hold off;
```

Listing B.8: Calculate the Fast Fourier Transform.

```
function [f, mag, angl] = calc_fft(data, Fs)

% Get the next power of two.
nfft = 2^(nextpow2(length(data)));

% Take the fft.
fdata = fft(data, nfft);

% Calculate the number of unique points.
NumUniquePts = ceil((nfft+1)/2);

% Throw away the second half.
fdata = fdata(1:NumUniquePts);

% Scale the magnitude by the length of the data vector.
mag = abs(fdata)/length(data);

angl = angle(fdata);

% Create the frequency vector.
f = (0:NumUniquePts-1)*Fs/nfft;
```

Listing B.9: Calculates the Fourier Coefficients.

```
function coeffs = fourier(signal)

N = length(signal);
M = (N-1)/2;

tmp = fft(signal)/N;

Xarray(1:M) = tmp(M+2:N);
Xarray((M+2):N) = tmp(2:(M+1));
Xarray(M+1) = tmp(1);

stem(0:M, abs(Xarray(M+1:N)));
coeffs = abs(Xarray(M:2*M));
```